NASA CR-159,308

NASA Contractor Report 159308

ANALYSIS OF ELECTRICAL TRANSIENTS CREATED BY LIGHTNING

J. E. Nanevicz

E. F. Vance

SRI International
333 Ravenswood Avenue
Menlo Park, California 94025

NASA

National Aeronautics and
Space Administration

Langley Research Center
Hampton, Virginia 23665

NASA Contractor Report 159308

ANALYSIS OF ELECTRICAL TRANSIENTS CREATED BY LIGHTNING

J. E. Nanevicz, Associate Director
E. F. Vance, Senior Research Engineer

Electromagnetic Science Laboratory
Technology and Systems Development Division

SRI International
333 Ravenswood Avenue
Menlo Park, California 94025

NASA
National Aeronautics and
Space Administration

Langley Research Center
Hampton, Virginia 23665

N80-30645

Page intentionally left blank

CONTENTS

ILLUSTRATIONS

v

TABLES

I INTRODUCTION

Background

Beginning in 1975, three flight test programs using the NASA Learjet have been carried out by SRI International to make a variety of electromagnetic measurements in the vicinity of Florida thunderstorms. In 1975, the program was initiated to support the launches of Apollo/Soyuz, Viking I, and Viking II by providing in-flight readings of electric fields above the launch pad beginning roughly 30 minutes before launch. For these tests, the aircraft was instrumented with a set of four field meters and a data processor to permit the resolution of the three components of static electric field at the aircraft location (unperturbed by the presence of the aircraft) and the aircraft potential. During the initial checkout and calibration of the aircraft and its instrumentation system, it was found that the Learjet with its instrumentation constituted an ideal vehicle for the study of the field structure in the vicinity of thunderstorm cells. Accordingly, arrangements were made for the Learjet to participate in a series of thunderstorm cell seeding experiments then under way at Kennedy Space Center (KSC), and to be used, when it was free, for target-of-opportunity flights around other thunderstorm cells. The results of the 1975 activity are described in Reference 1.[*]

In 1976, a second summer flight test program using the Learjet was planned, with primary emphasis on determining the electrostatic characteristics of the anvil structures associated with thunderstorm cells. This information was needed by NASA Johnson Space Center (JSC) in establishing launch and landing lightning safety rules for the forthcoming shuttle flights.

---

[*] References are listed at the end of the report.

The data from the 1976 electrostatic measurements were provided by SRI to NASA-JSC. A report describing the implications of these results on the Shuttle/Orbiter operation was prepared by NASA.[2]

To take advantage of the availability of the Learjet and its static field instrumentation in the summer of 1976, a modest, quick-reaction program was initiated by the Air Force to install suitable instruments on the Lear to permit simultaneous measurement of the electromagnetic transients associated with nearby lightning. The transient study program had a number of objectives that can be summarized generally as follows:

- Provide information regarding the lightning transient source from the vantage point of an aircraft.

- Study the interaction of the aircraft with its environment in the vicinity of thunderstorm cells.

- Measure signals induced by lightning flashes in wiring on the inside of the aircraft.

- Gain experience regarding the capabilities and limitations of modern instrumentation in making flight test measurements of lightning effects.

- Generate inputs and recommendations regarding the design of future tests.

- Assess the usefulness and limitations of ground-based measurements in describing lightning effects on aircraft.

For the electromagnetic transient studies of 1976, the instrumentation and sensors were quite rudimentary—one or the other of two measuring systems could be used to monitor signals induced in two sensors installed on the Learjet test aircraft. The first measurement system consisted of a pair of fixed-frequency spectrum analyzers covering the range 10 kHz to 30 MHz at half decade separations. The second measurement system consisted of a single-channel Tektronix R7912 transient digitizer provided and operated by AFFDL. Space limitations on the aircraft were such that both of the measuring instruments could not be carried on the aircraft at the same time.

Sensors for the 1976 transient measurements consisted of an electric dipole mounted roughly amidship on the top exterior of the aircraft, and a single wire strung roughly 4 inches from the skin in the cabin of the aircraft. With this combination of sensors and measurement systems, it

2

was possible to study electromagnetic signals on the exterior and the interior of the aircraft in either the time domain or the frequency domain. Results of the 1976 transient electromagnetic studies are given in a pair of reports: one by SRI describing primarily the spectrum analyzer measurements[3] and one by AFFDL concerned primarily with the transient digitizer measurements.[4]

1977 Learjet Program

When it was determined that Thunderstorm Research International Program (TRIP 77) would be under way at KSC during the summer of 1977, planning was initiated for a program involving the Learjet. With the experience of 1975 and 1976 to build on, it was possible to devise a highly productive program capable of being fielded in a short time at relatively modest cost. Flight testing during 1977 was designed to take advantage of any suitable supporting ground-based data that might be generated by TRIP experimenters.

The approaches to be taken in designing the instrumentation were determined through a review of the results of the earlier Learjet tests, together with descriptions of ground lightning characteristics[5] and studies of the coupling of signals through apertures into shielded structures[6] (also see Appendix A).

The results of the 1976 Learjet program indicated that a considerable amount of high-frequency energy is generated by activity occurring before the main high-charge-transfer portion of a lightning stroke. Because coupling through apertures is dominated by the higher frequency components of external signals, the observed precursor and early-time activity could be particularly important in inducing signals in internal aircraft wiring. Currently, the "standard stroke" waveform widely used for lightning noise calculations basically models the return stroke current and does not include signal components resulting from precursor activity. A major goal of the 1977 Learjet program was therefore to provide additional information on the high-frequency components of the lightning fields and on their contributions to internal transients.

The philosophy followed in designing instrumentation for the 1977 program was to provide additional information in areas not covered by earlier testing and to arrange the system in such a way that the load on the flight test observers was not significantly increased.

Acknowledgments

II AIRCRAFT INSTRUMENTATION

General

A review of the 1976 program indicated several areas in which substantial improvements and additions to the aircraft instrumentation would be desirable. First, it was observed that a lightning flash generates a complicated electromagnetic signal with components ranging from virtually dc to tens of MHz. Thus, to define the signal and to associate it with a particular flash, it is necessary that all measured data be recorded in such a way that accurate time correlation of all of the components is possible. Also, there are sufficient differences from flash to flash that a meaningful comparison of the outputs of different measuring instruments is greatly simplified if the measurements are made on the same flash--and even on the same components of a given stroke in the flash.

These measurement problems led to the requirement that all instrumentation be flown at the same time. It was also necessary to include an accurate clock in the instrumentation and to record the data in such a way that time correlations were possible. Ultimately, all of the data were recorded on an analog tape recorder and on floppy-disc storage. Also, an improved method for recording aircraft parameters was needed. The recording methods had evolved from penciled notes in 1975 to a voice log on a cassette recorder in 1976. Automated recording of outputs from the aircraft systems was needed in 1977 to free the observer to operate the additional instrumentation that was to be carried.

A review of the measured transient parameters indicated that additional sensors and different types of sensors should be installed on the test aircraft. This was necessary to assist in following the lightning transient through the various stages from propagating field to induced aircraft skin currents to noise signals on internal wiring.

5

Aircraft Instrumentation

The instrumentation system flown on the Learjet in summer 1977 is shown in block form in Figure 1. It should be noted that all of the instrumentation shown in the figure was installed in the aircraft and could be operated simultaneously in flight.

The spectrum analyzer systems were made up of individual fixed-frequency receiver channels of the sort used in 1976 and discussed in Reference 3. In fact, some of the channels were simply removed from the earlier instrumentation system and repackaged to require less space. The spectrum analyzer instrumentation was divided into four distinct systems labeled Spect. Anal. No. 1 through No. 4 in Figure 1. Provisions were included in the overall instrumentation to allow any of the spectrum analyzer systems to be used to monitor any transient sensor.

Spectrum analyzer systems No. 1 and No. 2 each incorporated four receiver channels covering the range 10 kHz to 30 MHz, whereas systems No. 3 and No. 4 each consisted of only two channels (300 kHz and 10 MHz). This was a compromise arrangement necessitated by the fact that the analog tape recorder available for the flight tests could accommodate only 14 data channels. Systems No. 1 and No. 2 could be used to obtain a reasonably detailed look at the signals in two of the sensors, and the availability of systems No. 3 and No. 4 made it possible to simultaneously monitor two other channels in a more abbreviated way. Although other groupings of channels might be possible, the one finally employed was a trade-off between obtaining detailed information from a limited number of sensors and obtaining only cursory information from a large number of sensors. In retrospect, it appears that it would have been preferable to duplicate the 30 MHz upper frequency of systems No. 1 and No 2, in systems No. 3 and No. 4.

Each stroke within a lightning flash is composed of a large number of components of widely varying spectral nature. To be able to define the nature of the lightning electromagnetic source, it is necessary to be able to resolve these individual components. For this reason, each of the spectrum analyzer channels was designed to have a 20 kHz bandwidth to take full advantage of the bandwidth capabilities of the analog

6
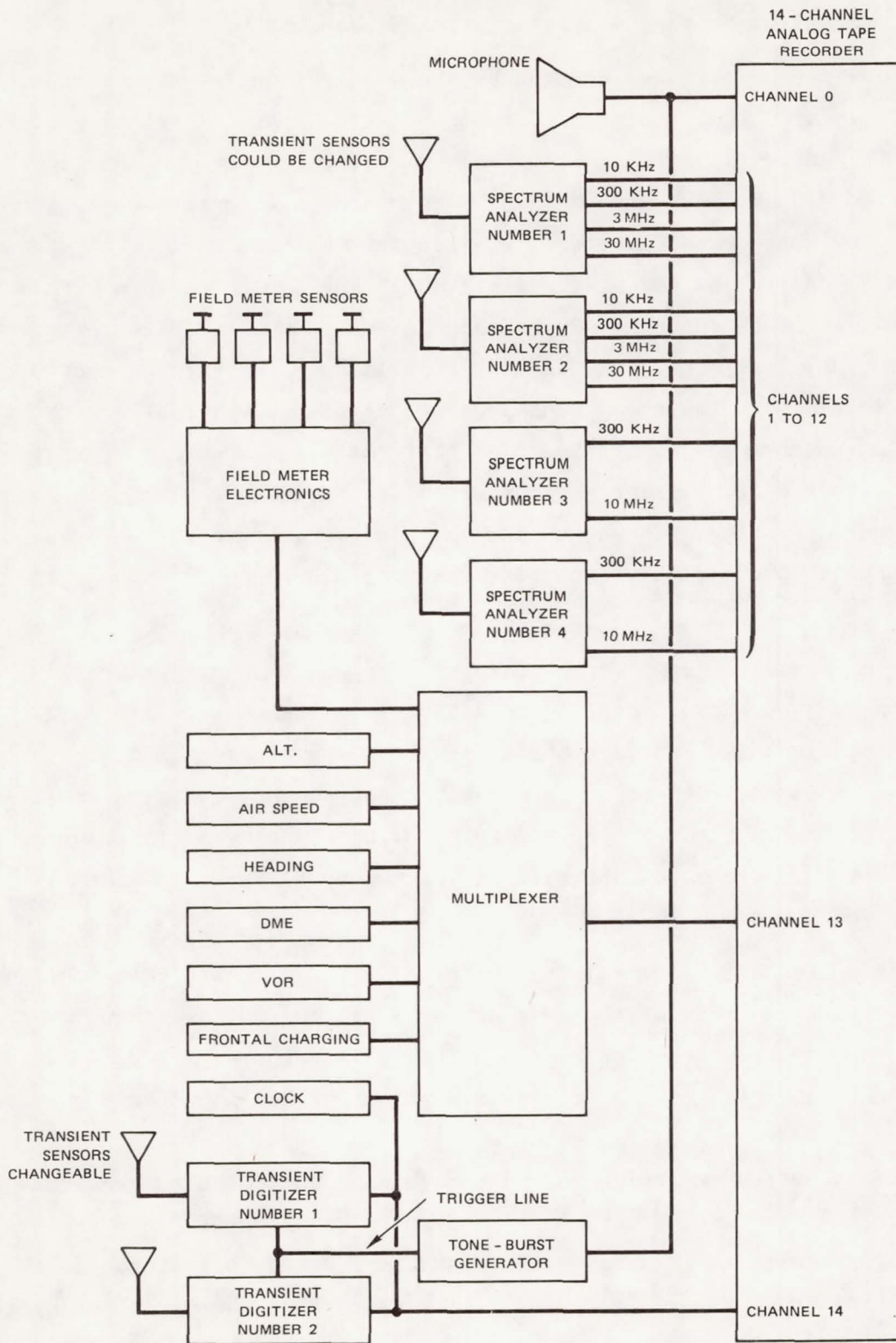
FIGURE 1   BLOCK DIAGRAM OF 1977 LIGHTNING TRANSIENT STUDY INSTRUMENTATION

tape recorder. Post-detection filter characteristics were also designed to be compatible with the available 20 kHz bandwidth.

The frequency range covered by the spectrum analyzers was chosen on the basis of a number of considerations. A substantial fraction of the spectral energy in a flash is contained in the low frequencies (10 kHz), and accordingly, much ground-based data has been generated using low-frequency monitors. Therefore, the Learjet spectrum analyzer system included provisions for measurements at 10 kHz for comparison with published ground-based data. Experience gained in nuclear electromagnetic pulse (EMP) analysis indicated that signals coupling through apertures in a shielded system are proportional to di/dt where i is the current flowing in the shield.[6] This means that the high-frequency processes in the stroke are extremely important in determining the signals induced in interior wiring. Consequently, the spectrum analyzer system was designed to include provision for measuring signal components up to 30 Mhz.

In general, the spectrum analyzer provides a means for breaking the lightning pulse down according to activity in the various frequency regimes. This is important because the time waveform of the lightning signal is dominated by the high-level, low-frequency signal associated with the return strokes. Accordingly, high frequency activity of great interest in determining aircraft system response is not prominently displayed on normal oscillograms.

Also shown in Figure 1 are two transient digitizers that could be connected to members of the same set of electromagnetic sensors used with the spectrum analyzer system. The digitizer system was similar to the unit flown on the Learjet in 1976 and described in Reference 4. Each digitizer channel is essentially a wide band (100 MHz or more) oscilloscope that is triggered by the leading edge of the transient, and writes the transient signal as a pattern on an array of diode cells. The stored pattern is subsequently read, processed, and stored in the floppy-disc memory of a computer making up part of the digitizer system.

In the early planning for 1977, SRI personnel thought that space and power limitations on the Learjet would preclude more than two digitizer

channels in the instrumentation system. Largely at the insistence of Boeing personnel, who indicated that they needed additional time domain data to be able to apply their computer codes to the analysis of transient coupling to the Learjet, an intensive packaging and power conservation effort was implemented. Through extensive repackaging, it was finally possible to install in the Learjet all of the instrumentation shown in Figure 1, plus two additional digitizer channels. Once flight testing started, however, it was found that the Learjet air conditioner could not cool the cabin adequately when even two digitizers were on. This was true even when special air hoses to direct cooled air to the digitizer installation were used, and it was necessary to use blocks of dry ice to provide adequate overall cooling. For essentially all of the flight test program, therefore, the instrumentation complement of Figure 1 was actually used.

The provisions used for time correlation of the digitizer and spectrum analyzer data are shown in the lower part of Figure 1. A binary coded decimal (BCD) time signal was recorded by the PDP-11 computer for each digitizer system trigger, while a continuous IRIG B time code signal was recorded on one of the analog tape recorder channels used in conjunction with the spectrum analyzer. In addition, digitizer firings were marked on the spectrum analyzer record by firing a tone burst generator using the digitizer trigger signal. The tone burst was recorded on the voice log channel of the analog tape recorder.

All of the low-bandwidth data were multiplexed onto a single channel of the tape recorder. These data included outputs from the field-meter system; aircraft parameters such as altitude, heading, etc.; and the frontal charging current generated by flight through precipitation.

The field-meter system was essentially the same as that flown on the Learjet in 1975 and 1976.[1] In addition to recording the outputs from the data processor that yields the free-space field components E_x, E_y, and E_z provisions were made to record data from the individual field meter sensors. In this way, important data could be salvaged even if the data processor is overloaded or inoperative during a portion of a

9

flight. Gain settings of the field-meter processor were also recorded as part of the multiplexed data so that the observer was free to change gain as appropriate without having to worry about maintaining a log.

Aircraft parameters were derived largely from existing systems on the aircraft. Synchro-to-dc converters provided by NASA-JSC were used to convert aircraft signals into analog dc signals for inclusion in the multiplexed data.

The frontal charging measurement system consisted of an electrically isolated metal patch with a frontal area of 222 cm^2 (34.5 inches^2) mounted on the nose of the right fuel pod. Charging current generated by precipitation particles impinging on this patch flowed to the airframe through the input stage wiring of a dc amplifier located immediately behind the patch. The output of this amplifier was fed to the multiplexing system and recorded. Frontal charging information is of interest in that it provides a sensitive indication of when the aircraft was operating in a cloud. The magnitude of the current is related to the precipitation particle concentration within the cloud.

The voice track on the tape recorder was used to further minimize the amount of log keeping required in flight. Provisions were made to record all of the voice activity on the aircraft intercom system. Recordings were made of pilot, copilot, and experimenter comments and of radio transmissions.

Sensors

In 1977, the Learjet carried a wide variety and large number of sensors. The sensors that protruded through the aircraft skin are shown in Figure 2. Five field meters were installed as shown. The two wing tip units and the two fuselage units were connected to the analog data processing system. The output of the field-meter sensor in the fin cap was recorded directly to serve as a backup if one of the other field-meter sensors failed at a critical time. The field-meter system measured the ambient static electric field at the aircraft location. In addition, this system provided an indication of the static field change resulting

10
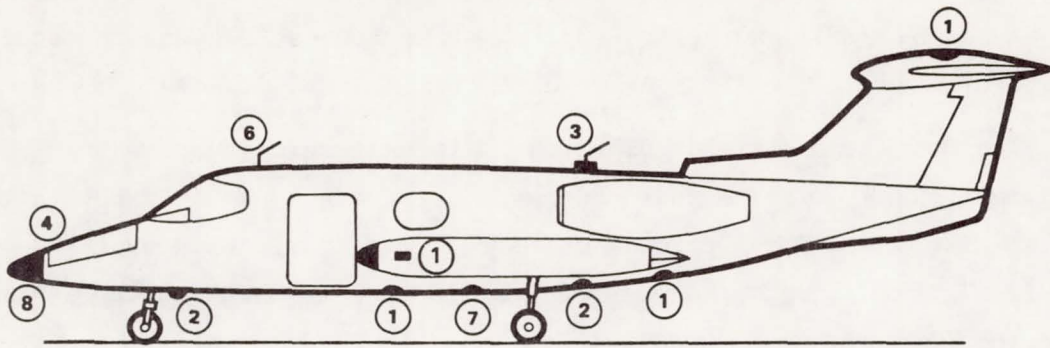
1977 LEARJET EQUIPMENT LIST

(1) FIELD MILLS (5 each)
(2) SKIN - CURRENT SENSORS (4 each)
(3) E - FIELD ANTENNA
(4) H - FIELD ANTENNA
(5) CHARGING PATCH
(6) W.W.V. ANTENNA
(7) C - BAND BEACON
(8) DIGITAL WEATHER RADAR
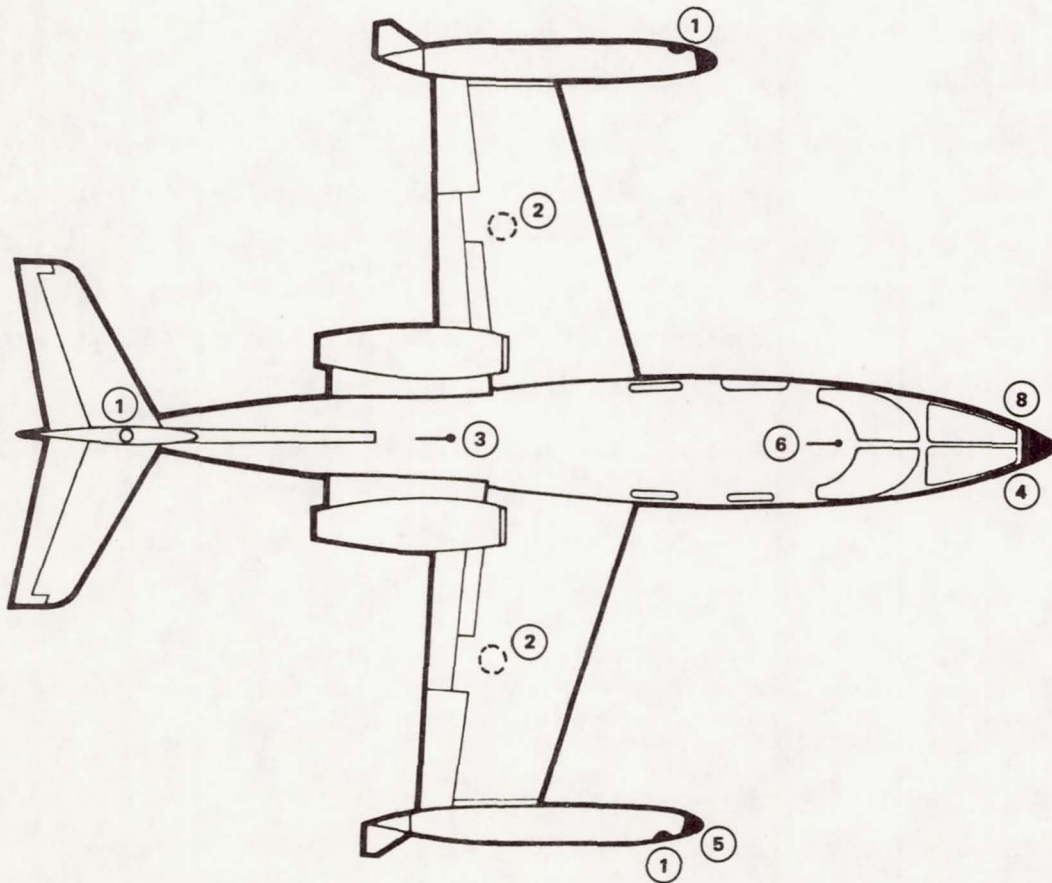
FIGURE 2   SENSORS MOUNTED IN SKIN OF AIRCRAFT

11

from the neutralization of charge during a flash. This change takes place over a period of the order of a second and can be used to obtain a rough estimate of the distance to a flash.

The propagating field generated at the aircraft location by a lightning flash could be measured by two separate sensors on the exterior of the aircraft. The first was an E-field antenna located on the top of the fuselage and the second was an H-field loop antenna mounted in the nose radome.

The E-field antenna was a 24-inch-long whip mounted on an existing antenna feedthrough insulator. To measure transient electromagnetic signals, it is necessary that the receiving antenna be either very long and resistively loaded or that it be short compared with the highest wavelength of interest. With a short antenna, the ringing introduced by reflections from the ends of the antenna is designed to be beyond the pass band of the measuring system so that the ringing does not show up in the measurements. The 24-inch-long wire used was chosen as being sufficiently short for the intended measurements.

A short dipole antenna has the equivalent circuit shown in Figure 3.[7] For a highly top-loaded dipole, the effective height, h_e, is equal to the physical height of the antenna. For antennas with other physical forms, both h_e and antenna capacitance, C_A, generally must be determined by measurement. The values of the parameters of the Learjet antenna were determined from the experimental data of Reference 7.

If the antenna is capacitively terminated, then the terminal voltage is directly proportional to the ambient field E:

$$V_{out} = k \, h_e \, E(t) \quad . \tag{1}$$

(With a resistive termination, the output voltage will be proportional to the derivative of the field.)

For the flight tests, the parameters of the input circuitry were chosen so that the load resistance, $R_L \gg 1/\omega C_L$ down to the lowest
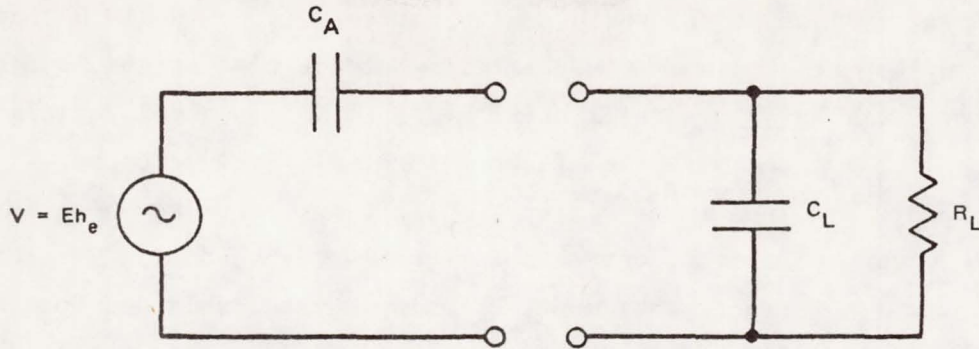
FOR LEARJET ANTENNA

$h_e = 0.17$ m

$C_A = 7.8$ pF

FIGURE 3   EQUIVALENT CIRCUIT OF SHORT ELECTRIC DIPOLE

frequencies of importance, and so that signals directly proportional to the ambient electric field at the antenna location were applied to the input of the transient digitizer and spectrum analyzer.

Although the electric dipole antenna was suitable for measuring the propagating electromagnetic field, it suffers from being influenced by sudden changes in aircraft potential caused by triboelectric charging.[8] A magnetic loop is much less susceptible to triboelectric charging provided that it is mounted on an extremity, such as the nose of the aircraft, away from the noise sources.[9] A loop mounted at the nose is also highly decoupled from the currents flowing on the fuselage so that it responds primarily to the propagating H-field and can therefore be used as a sensor for free-space field measurement.

In general, it is not possible to obtain both early time (20 ns) and late time (ms) data with one sensor because this implies a 50,000:1 bandwidth. A loop differentiates at low frequencies unless L/R is made large ($\approx 10^{-3}$ sec), but then the high frequency (HF) response is poor because of resonances in L. Loop response to H is good if L/R is small (20 ns), but the late time field cannot be retrieved because H is then too small at late times.

13

After considering the various alternatives, it was decided that a multiturn loop responding to the H-field would be used at the nose of the aircraft. The 45 cm (major axis) by 39 cm (minor axis) semielliptical nose loop antenna was made of three turns of 12-gauge copper wire shielded by a 3/8 inch inner diameter solid copper tube as shown in Figure 4. Induced antenna currents were measured by using a Tektronix type CT-2 current transformer mounted inside a small shielded box. This box was symmetrically located on one side of the loop immediately opposite the small break inserted in the copper shield. The transformer output was fed through a BNC-type feedthrough connector to the instrumentation by coaxial cable. The parameters of the antenna are such that it operates as a true H-field antenna over the range 4 kHz to 70 MHz (3 dB points).*

In considering the response of an airborne system to lightning transients, it is convenient to break the problem up into several steps. First, the propagating field induces currents and charge displacements on the airframe. These airframe currents excite apertures or diffuse through the skin to generate fields that induce currents in wiring on the interior of the aircraft. To assist in the analysis of this problem, the Learjet was equipped with a set of skin current sensors as shown in Figure 2 to help define the way in which the airframe is excited by the lightning fields. Originally, it was planned that only two skin current sensors (one on the fuselage and one on the wing) would be used, but Boeing personnel indicated that their analysis of the Learjet would be compromised unless four sensors were available.

At the surface of a good conductor, the magnitude of the tangential magnetic field intensity, H, is numerically equal to the magnitude of the surface current density, J. Thus, the sensor for the skin current density may be either a magnetic dipole (small loop) or a current

---

*This antenna was mounted on the inner wall of the Learjet radome, and thus its in-site sensitivity and frequency response were somewhat affected by the nearby metallic support mount for the radome and weather radar antenna (see Appendix B).

14
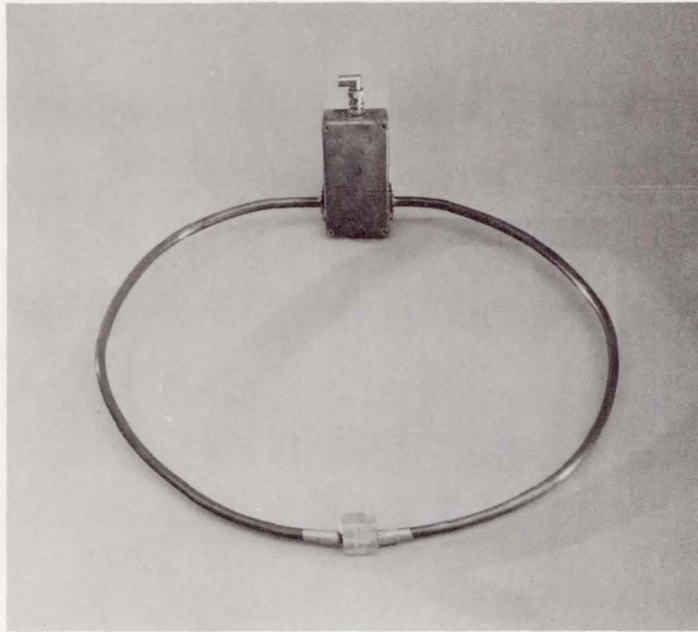
(a) PHOTOGRAPH OF ASSEMBLED SENSOR

THREE TURNS OF
NUMBER 12 AWG
COPPER WIRE

CURRENT TRANSFORMER

SHIELDED BOX

SHIELD BREAK

LUCITE SPACER

BNC OUTPUT

SOLDER FLANGES

3/8" I.D.
COPPER TUBING
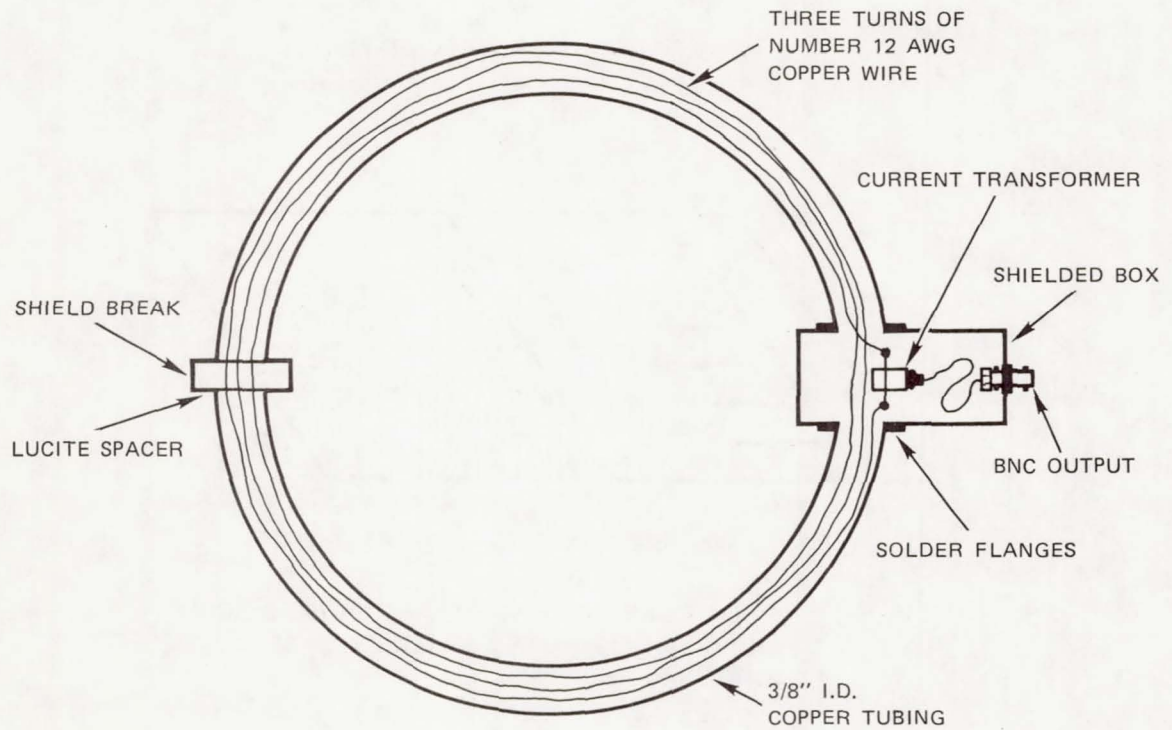
(b) SENSOR ELECTRICAL DETAIL

FIGURE 4   H – FIELD ANTENNA CONSTRUCTION

dipole (small slot). As illustrated in Figure 5(a), the loop antenna responds to the magnetic field at the surface of the conducting plane if the elementary flux linkage concept is used, but the loop antenna may also be considered to respond to the current induced in the plane by the magnetic field. In the dynamic field case, the current in the ground plane and the surface magnetic field are inseparable. An elementary concept of the slot antenna of Figure 5(b) may be obtained by considering that the slot interrupts the uniform current density, J, that would normally flow on the surface, forcing part of this current to flow
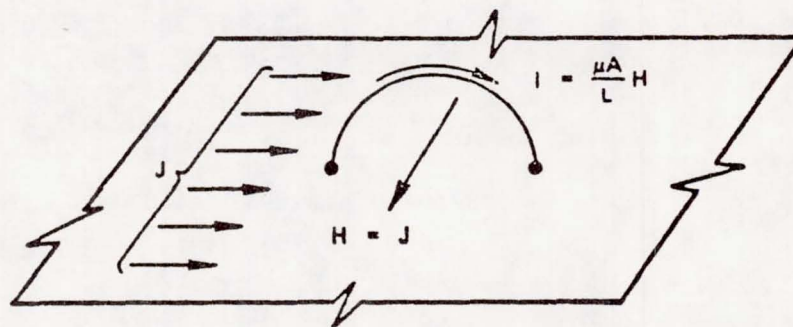
(a)   HALF-LOOP OVER GROUND PLANE
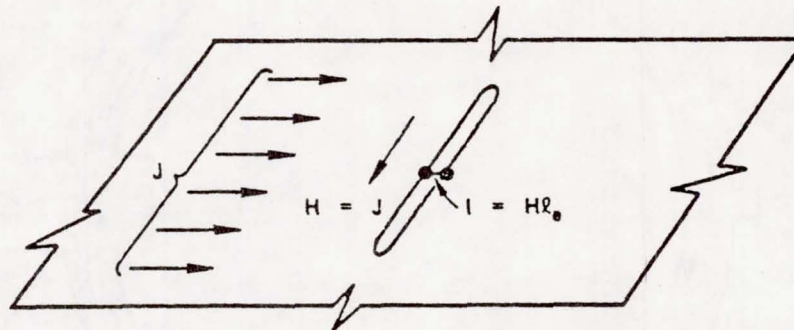
(b)   SLOT IN GROUND PLANE

FIGURE 5   FIELD, CURRENT DENSITY, AND SHORT CIRCUIT
CURRENT RELATIONS FOR LOOP AND SLOT
ANTENNAS

through the short-circuited slot terminals. The short-circuited slot current is

16

$$I = J\ell_e = H\ell_e \quad . \tag{2}$$

The impedance of the small slot is primarily inductive reactance. Hence, the open circuit voltage at the slot terminal is

$$V = \ell_e L \frac{dJ}{dt} = \ell_e L \frac{dH}{dt} \quad . \tag{3}$$

The short-circuit current and open-circuit voltage of a small loop antenna are

$$I = \frac{\mu A}{L} J \quad \text{and} \quad V = \mu A \frac{dJ}{dt} \quad , \quad \text{respectively} \quad , \tag{4}$$

where A is the area of the loop, $\mu = 4\pi \times 10^{-7}$ H/m, J is the surface current density, and L is the loop inductance.

To make the loop insensitive to the electric field, it is necessary to shield the loop. Conventional shielded loop design (in which the loop is fabricated as a semicircle of coaxial cable over a ground plane with the center conductor grounded at one end and the shield grounded at one end) was used for the skin current sensors on the fuselage. These sensors are more sensitive than are slots of comparable size, but they protrude from the skin. On the fuselage, the plane of the loop is parallel to the airstream when the loop is oriented to respond to the current flowing along the fuselage. To respond to the current along the wings, however, the plane of the loop would be oriented broadside to the airstream. Hence, on the wings, slot sensors that are flush with the skin were used. Photographs of the skin current sensors are shown in Figure 6.

To measure the short-circuit current, the current measuring apparatus must have an impedance that is small compared with the inductive reactance $j\omega L$ throughout the frequency range of interest. Because L is small for a small half loop and even smaller for a small slot, it is difficult to measure the short-circuit current directly (the commonly used current probes have insertion impedances of the order of 1 ohm in parallel with

17
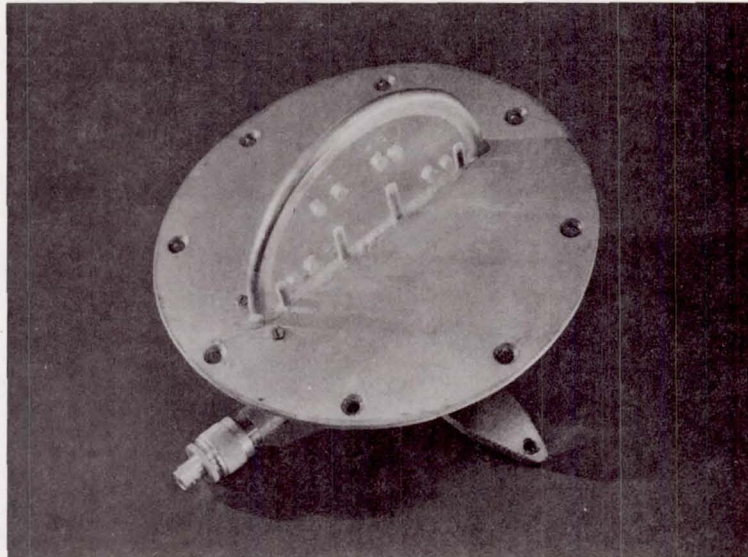
(a) HALF LOOP
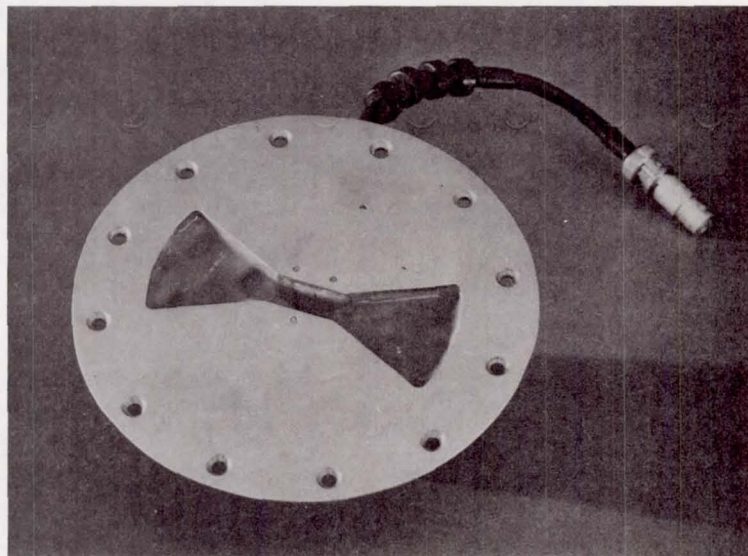
(b) SLOT

FIGURE 6   SKIN CURRENT SENSORS

18

several tenths of a μH). Therefore, the open-circuit voltage is usually measured. A 50-ohm coaxial cable may be connected directly to the terminals of either the slot or the loop, and for frequencies such that

$$f \ll \frac{50}{2\pi L} \quad , \tag{5}$$

the voltage delivered to the coaxial cable is approximately the open-circuit voltage. This method was used for the Learjet skin current sensors.

The calibration factors for the skin current sensors are thus of the form

$$\dot{J} = \frac{dJ}{dt} = \frac{V}{\ell_e L} \text{ (slot)} \quad . \tag{6}$$

$$\dot{J} = \frac{V}{\mu A} \text{ (loop)} \quad . \tag{7}$$

For the loop sensors, the value of $1/\mu A$ is calculable from the dimensions of the loop. Thus $1/\mu A = 196 \times 10^6$ (H-m)$^{-1}$ for the circular half-loop with a 2 inch (0.051 m) radius.

The calibration factor, $1/\ell_e L$, for the slot sensor was determined from measurements in a rectangular coaxial transmission line (see Appendix B). The slot calibration factor is

$$\frac{1}{\ell_e L} = 912 \times 10^6 \text{ (H-m)}^{-1} \quad . \tag{8}$$

The bandwidth of the loop sensor with 50-ohm load is

$$BW = \frac{R}{2\pi L} = \frac{50}{2\pi L} = 87 \text{ MHz} \tag{9}$$

for the calculated loop inductance of 91 nH. The inductance of the slot is much smaller than that of the loop, so the bandwidth of the slot is much greater than the bandwidth of the loop.

19

The frontal charging current patch mounted on the nose of the right wing tip tank is illustrated in Figure 7. Figure 7(a) shows the sensor as seen from the exterior of the aircraft. Figure 7(b) shows the circuitry, which consisted of an operational amplifier to provide impedance transformation between the high-impedance current source characteristics of the sensor, and the input source impedance required by the multiplexer.

Because the charging patch was mounted far from the fuselage and well forward of the wing, the patch sampled essentially undisturbed conditions. The absolute dimensions of the sensor were chosen to be small so that its effective intercepting area could be taken to be equal to its projected frontal area. (Aerodynamic influences on precipitation particle impact as they apply to precipitation charging are discussed in References 10 and 11.) The intrinsic charging current density can be determined by dividing the measured current by the projected frontal area of the patch ($A_f = 0.24$ ft^2). In earlier flight tests for precipitation static studies, it was found that intrinsic charging current density ranged from roughly 10μA/ft^2 in light cirrus to 40μA/ft^2 in frontal snow.[8-11]

The WWV antenna shown in Figure 2 was installed to be used with a receiver to synchronize the aircraft clock with the WWV timing signals. The WWV antenna consisted of a short whip antenna mounted on an existing feedthrough insulator.

A C-band antenna and beacon system was installed on the aircraft to enable it to be tracked from the ground when operating over KSC.

For the current program, the normal weather radar was replaced by a modern digital weather radar incorporating a three-colored display. The availability of such a radar system simplifies the problems associated with operating near thunderstorm cells without inadvertently penetrating into highly turbulent regions.

(a) PHOTOGRAPH OF SENSOR
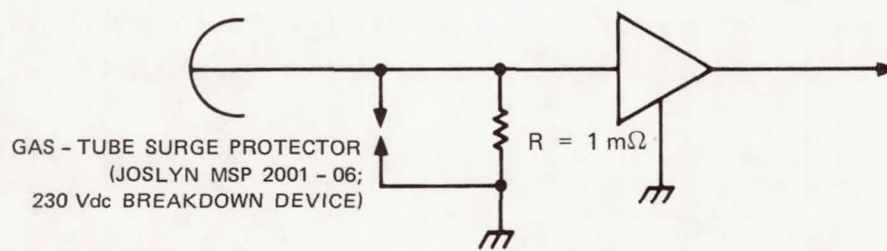
(b) FRONTAL CHARGING SENSOR CIRCUITRY

FIGURE 7   CHARGING CURRENT PATCH MOUNTED ON NOSE OF RIGHT WING TIP TANK

21

In addition to the external sensors discussed in connection with Figure 2, the Learjet incorporated a number of instrumented wires* on its interior, as shown in Figure 8 and listed in Table 1, that could be used to measure the signals induced on typical cabling on the interior of the aircraft. The first such wire was installed inside the cabin in the same general manner as it was in the tests of 1976.[3,4] This sensor was included in the instrumentation complement to provide a common measurement to help tie together the 1976 and 1977 measurement programs.

The remaining pickup wires shown in Table 1 were installed in the major members of the airframe. Because each one couples electromagnetically primarily to currents flowing on the member in which it is installed, the cable current measurements provide a technique for investigating the coupling between airframe skin currents and wiring on the interior. The locations of the wires and their number were determined by the simple expedient of running two extra wires in each bundle leading from the cabin to each of the field-meter sensors. One of the wires in each pair was shorted to the airframe at its field-meter sensor location. The second wire of each pair was terminated with a 68-ohm resistor (which was a rough estimate of the wire's characteristic impedance) at its field-meter sensor location.

A patch panel inside the cabin permitted the special sensor wires to be terminated in either a short circuit or the characteristic impedance of 68 ohms. Tektronix CT-2 current transformers (Z_T = 1 mV/mA) were used to measure the termination current in wires of interest.

In general, the spectrum analyzers and the transient digitizers could be connected to any of the external or internal sensors. Power splitters mounted in a patch panel in the cabin allowed selected sensors to be monitored simultaneously by both a spectrum analyzer and a digitizer.

---

*Ordinary No. 20 hook-up wire was used for this purpose, e.g., Alpha No. 1553-20-10/30 PVC type MW-V (Mil. No. W-76B).

22
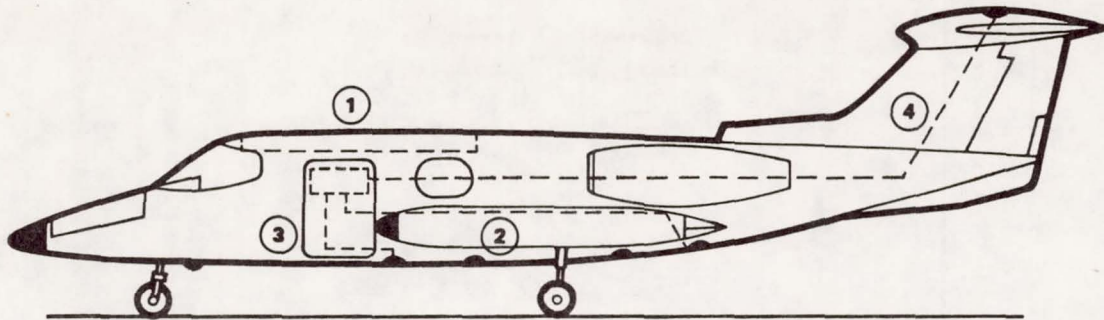
1977 LEARJET EQUIPMENT LIST

(1) CABIN WIRE
(2) AFT FUSELAGE
(3) FORWARD FUSELAGE
(4) FIN CAP
(5) RIGHT WING
(5A) RIGHT WING (after 8/18/77)
(6) LEFT WING
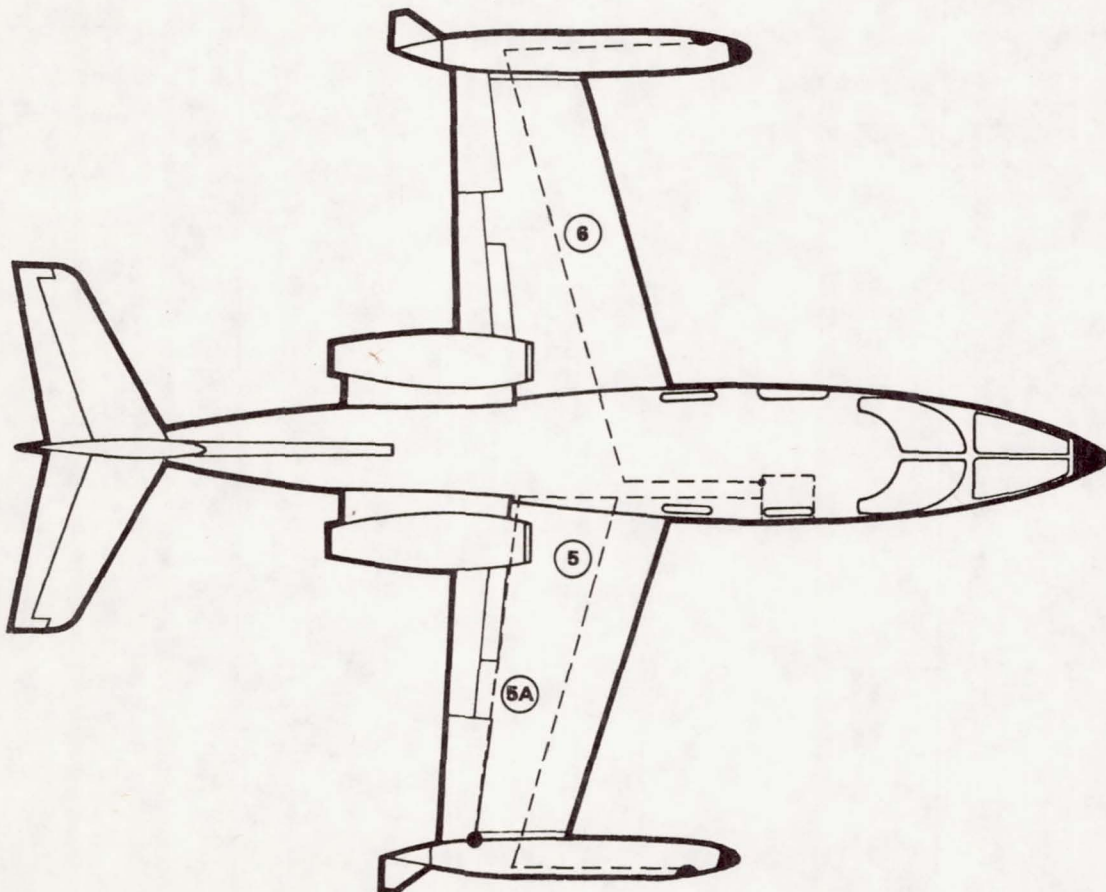
FIGURE 8 WIRE PICKUP SENSORS ON INTERIOR OF LEARJET

23

Table 1

WIRE PICKUP SENSORS
ON INTERIOR OF LEARJET

Designation	Length (meters)
Cabin wire	3.58
Aft fuselage	7.2
Forward fuselage	3.8
Fin cap	14.3
Right wing	12
Left wing	13

Sensor and System Calibrations

Various tests and calibrations of the individual sensors and sub-systems were carried out during instrument fabrication and throughout the flight test program. The calibration procedures and philosophies applied during the program are discussed in Appendix B.

III   FLIGHT TEST PROGRAM

A broad chronology of activity involving the Learjet is given in
Table 2 below:

Table 2

CHRONOLOGY OF ACTIVITY ASSOCIATED WITH LEARJET
701 DURING SUMMER 1977 LIGHTNING TESTS

Date	Comments
16 July	Shakedown flight at NASA-Ames.
17 July	Learjet arrives at Patrick AFB.
18 July	SRI personnel arrive at Patrick AFB. Air Force personnel arrive at Patrick AFB.
19-22 July	Working on test instrumentation and aircraft-- primarily digitizers, analog tape recorder, aircraft fire warning system.
23 July	Check-out flight--no good thunderstorms, but checked out field-mills and aircraft parameter measurements.
25 July-19 August	Test flights. Ground activity between flights to refine instrumentation.
20-28 August	Ground tests on aircraft--both low-power CW and high-power pulsing to investigate coupling to interior.
29 August-2 September	Test flights.
4 September	Voyager 1 launch support--not needed--clear day.

In general, the weather in Florida in the summer of 1977 was very
disappointing. Normally, beginning in the early afternoon and extend-
ing to early evening, numerous individual thunderstorm cells can be
found within the range of the Learjet. Individual cells are desirable
because close approach to the cell is possible (the air is clear

immediately outside), and the resulting electromagnetic/electrostatic data are dominated by processes occurring within that particular cell.

In the past, the operating procedure was to locate several newly developing cells immediately after takeoff, and to monitor their development as the aircraft approached their general area. The one showing the best development and promise would ultimately be selected for study. In summer 1977, individual cells formed very infrequently. Furthermore, it was found that when single cells could be located, most of the time they did not develop sufficiently to produce appreciable lightning. Thus, substantial flight time was spent working with cells that ultimately did not mature.

Much of the testing in 1977 was done in the vicinity of extended storms containing numerous cells. Close approach and study of a single cell is not possible in such a situation. Turbulence in the regions between the cells can be severe, and aircraft maneuvering to make successive passes is greatly complicated by the presence of nearby cells. As a result, most of the testing in 1977 was carried out with the aircraft substantially farther from any individual cell than was true in the past, and with other active cells in closer proximity than was true in the past.

During the entire test program, care was exercised to verify functioning and calibration of the flight instrumentation. Complete calibration and/or functional checks were carried out before and after each flight. The post-flight calibrations were usually carried out as soon as the aircraft became available after landing to allow as much time as possible to correct any problems discovered during the calibration. A data stripout facility was available at the test site throughout the program to allow a review of data as it was generated. All of the flight data were stripped out and reviewed (shortly after each flight) by SRI personnel at Patrick AFB.

IV FLIGHT TEST RESULTS

General

In general, all electromagnetic interference (EMI) problems can be
separated into the consideration of a source, the coupling mechanisms,
and the victim. In the case of an aircraft flying in the vicinity of
active thunderstorm cells, one can consider that the lightning source
excites currents and charge displacements on the wings and fuselage of
the aircraft, which in turn couple energy to interior wires connected
to the victim systems.

In undertaking the 1977 Learjet lightning experiments, the principal
objectives were to enhance knowledge of typical lightning processes
constituting the source and to obtain flight data on the coupling of
electromagnetic energy to the aircraft's exterior and interior. Pro-
visions were included in the instrumentation system to provide informa-
tion on the lightning source characteristics, the aircraft skin currents,
and ultimately the currents induced in interior wiring. The data were
recorded using both time-domain and frequency-domain instrumentation.

Unusual weather conditions in Florida during summer 1977 produced a
paucity of mature storms in the July-August period and affected the
logical flow of the experiments. Only 5 or 6 days from the 30 days of
flight time provided any significant lightning signatures. Also, as
was indicated earlier, when thunderstorms were available for study, they
often occurred in jagged strings of cells rather than as individual
developing cells. To avoid the risk of inadvertently flying through a
cell in the string, the aircraft was flown clear of the clouds--several
kilometers from the visible edge. (In 1976, it was normal procedure to
touch the cell wall with the wing tip on the closest approach, with the
result that the aircraft tracks passed within 4 to 5 km of the cell
center.) In 1977, however, most of the tracks were probably not closer

than 6 to 8 km of the cell center. Because of the conditions, localization of a lightning strike to a particular cell and normalization of source terms to a standard distance are not possible from the 1977 data.

In spite of these difficulties with the weather, however, important characteristics of lightning were identified and significant insights were obtained on the electromagnetic environment that aircraft and their avionic systems will experience near lightning storms. For example, much of the radiated high-frequency energy (10 MHz to 30 MHz) was determined to be associated with processes that occur before the major return current flow that neutralizes the charge centers in storm cells. Also, great variations exist in the spectral content from flash to flash and even from events associated with the same flash. For electromagnetic noise specification, the concept of a standard stroke may therefore have meaning only in a statistical sense. For example, in some cases, currents of the same order of magnitude were induced on internal cabin wires by sources both near to and far from the aircraft.

Two distinct classes of events make up the data base for this report: "near" lightning strikes and "far" lightning strikes. Sources termed "near" lightning strikes are those in which the RF signal from a flash is accompanied by a change in the electrostatic field. (As is indicated in Appendix C, the electrostatic term in the expression for the electric field near a storm falls off as $1/d^3$ with distance d from the storm, so that this term is significant only very near to the storm cell.) The sources termed "far" lightning strikes are identified with the presence of RF energy on one or more the sensors, but with no accompanying changes in the electrostatic field (i.e., the quasi-static term has decayed to zero). The ratio of near to far events examined for this report is approximately one to three. The terms near and far are meant only to indicate the presence or absence of an electrostatic field change and should not be inferred as signifying a great range of distances between the aircraft and the source. Indeed, the electrostatic field changes of the near events are small (in the 1 kV/m to 2 kV/m range) compared with the results of the 1976 program in which field changes of tens of kV/m were common. Because these small changes are accompanied by small initial static field magnitudes, it is believed

that the small changes are the result of greater distances between the aircraft flight track and the storm cells (see Appendix C). This interpretation is consistent with time-domain measurements of the radiated fields from the transient digitizer, which typically measured peak field strengths of a few tenths of a kilovolt per meter.

Figure 9 is an example of test data generated during the flights. This example is taken from the analog tape record of 10 August 1977 and provides good insight into the functioning of the Learjet instrumentation, demonstrates some of the properties of lightning, and illustrates some of the difficulties associated with lightning measurements.

The record shows all of the electromagnetic/electrostatic data recorded on the analog tape as a function of time. The top trace displays time coded in the IRIG B convention, and also indicates the gain setting of the field-meter-processor electronics. Field-meter calibrations corresponding to the "gain 2" and "gain 3" settings are shown at the right edge of Figure 9. The three components of electrostatic field are displayed as the three widely varying traces in the central portion of the record. The coordinate convention and field polarity convention followed in the program are shown in Figure 10. Basically, the standard atmospheric electrician's convention of associating a positive reading of potential gradient with a positive charge in front of the sensor was followed. (This is opposite to the normal sign convention for electric fields.) The bottom trace in the record is the crew's voice track filtered to accentuate the 3,000 Hz tone bursts generated each time the digitizer was triggered. Five such bursts are seen to have occurred in the period covered in the figure. Also, multiplexed on the bottom trace is the output of the precipitation charging patch located on the front of the right wing tank. The zero deflection of this trace indicates that the aircraft was not experiencing precipitation charging during the time covered in this record. Frontal charging information helps in distinguishing between far lightning sources and locally-generated noise stemming from aircraft electrical charging.

The remaining traces in Figure 9, and in all other records in the report, are reserved for spectrum analyzer outputs associated with

29
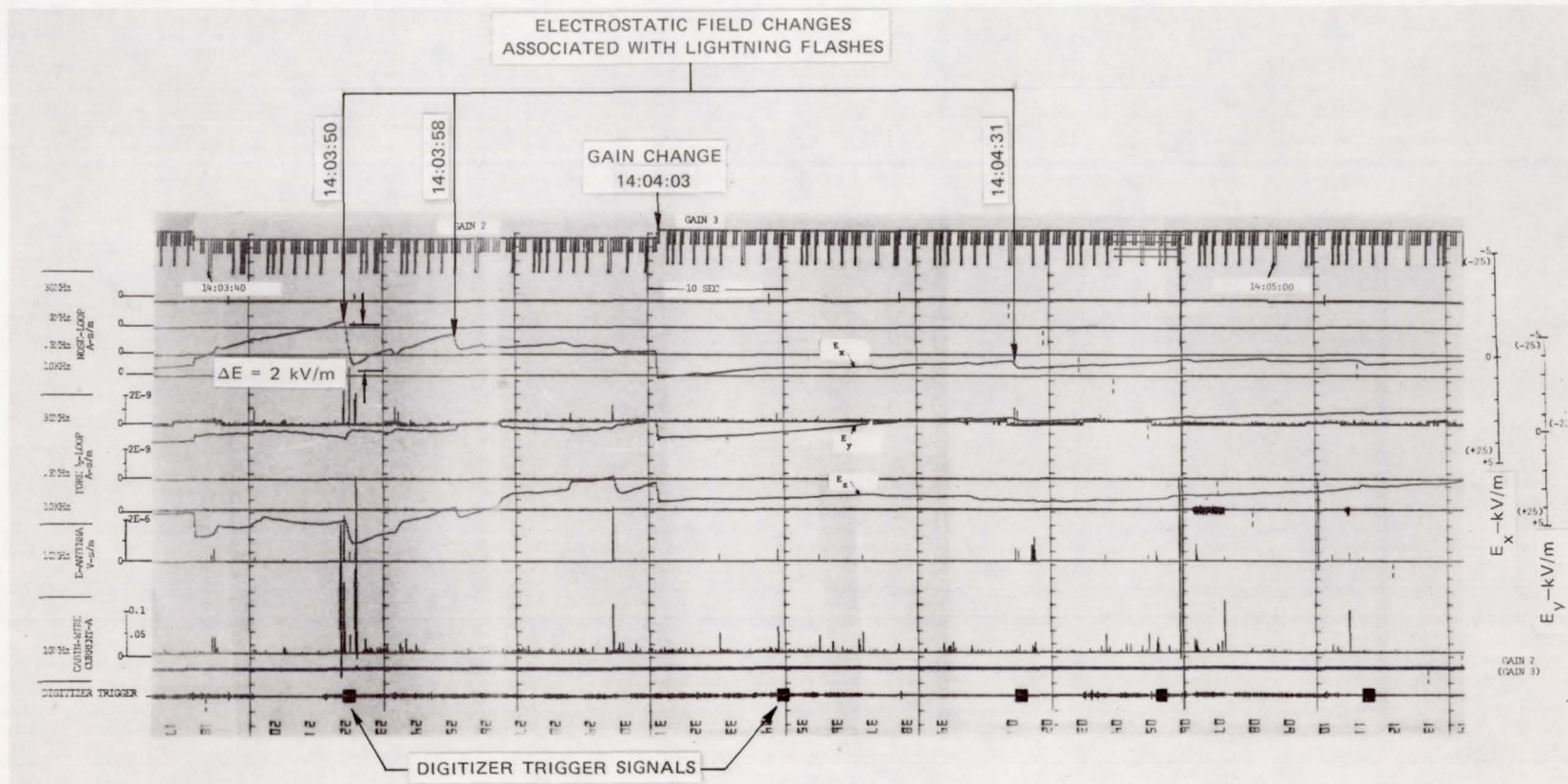
NOTE: Data from flight of 10 August 1977.

FIGURE 9   SAMPLE OF DATA RECORD FROM ANALOG TAPE RECORDER

30

SA-5537-24

(a) COORDINATE CONVENTION

CLOUD OF POSITIVE CHARGE

FIELD - METER OUTPUT

FIELD METER

AIRCRAFT
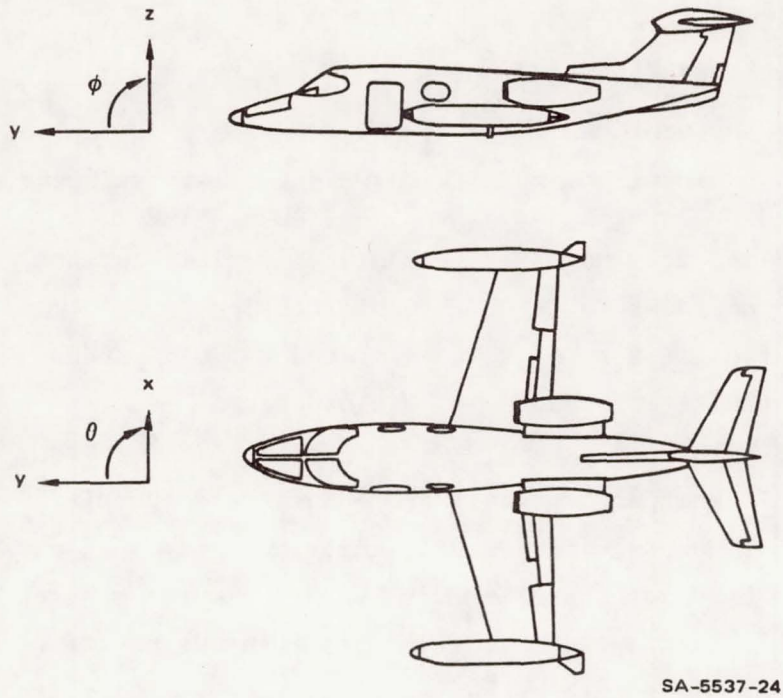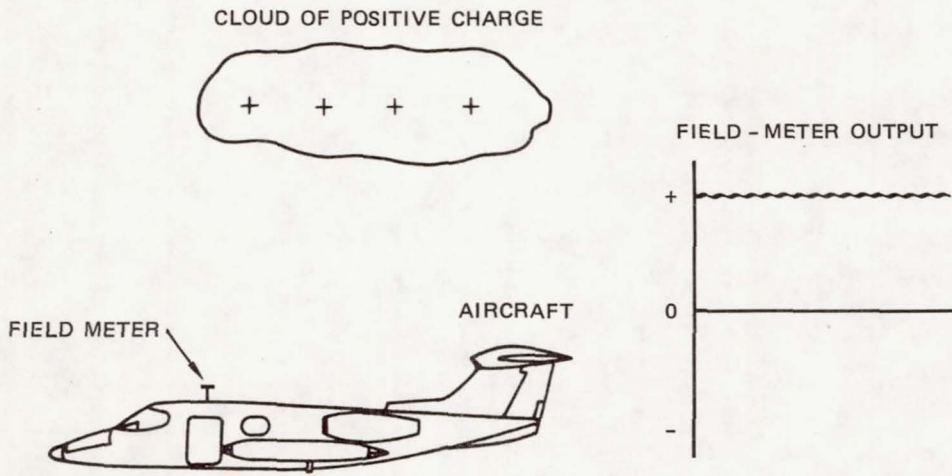
(b) POLARITY CONVENTION

FIGURE 10   THE COORDINATE CONVENTION AND POLARITY CONVENTION USED

31

various configurations of electromagnetic sensors. The interconnection
of sensors and instrumentation for this flight was as follows:

Instrumentation	Sensor
Spectrum analyzer No. 1	H-field antenna (nose loop)
Spectrum analyzer No. 2	Forward fuselage skin current (forward half-loop)
Spectrum analyzer No. 3	Radiated E-field antenna
Spectrum analyzer No. 4	Cabin wire current
Transient digitizer No. 1	Radiated E-field antenna
Transient digitizer No. 2	Not connected

The outputs of the specturm analyzer channels are identified on the
right side of Figure 9. In general, the record for each channel is
characterized by a zero baseline with upward excursions each time an RF
signal occurs. Each spike actually represents the positive detected
envelope of the signal present at each discrete analyzer frequency. When
this record was made, two of the spectrum analyzer channels were not
functioning and are not shown on the record. These are: SA No. 2,
3 MHz channel (forward fuselage skin current) and SA No. 3, 0.3 MHz
channel (radiated E-field antenna).

Various interesting features are shown in Figure 9. The electro-
static field changes in the record indicate the occurrence of lightning
flashes from a near source. Typical static field relaxation times are
on the order of 0.5 to 1.0 second. The particular static field com-
ponent most affected by the lightning discharge varies from flash to
flash in Figure 9 indicating that different charge centers are involved
in successive flashes. The lightning events occurring at 14:03:50 and
14:04:31 show sequences of RF activity in which many spectrum analyzer
pulses both precede and follow the change in the electrostatic field
component. (The apparent step in the field components at 14:04:03 is an
artifact from changing the field-meter processor gain.) However, at
14:03:58, a static field change occurs with no accompanying RF response
recorded on the E-field antenna, forward half-loop, or cabin wire.

32

Apparently, the RF signals were too small to cause a deflection in the record.

In general, it is evident that there is a substantial variation in spectral amplitude and distribution from flash to flash. Some of the gross differences in the generated signals are a natural result of differences in the radiation source, viz., cloud to ground, or intercloud strike. Even for a particular type of source, it is reasonable to expect significant differences in the RF signal character because much of the energy is produced by complicated leader processes preceding the main return current. Another factor important in explaining differences in RF signature from flash to flash is the orientation of the aircraft and sensors with respect to the lightning source.

Typical Data Outputs

A series of events from the flights of 10 August and 29 August recorded both on the spectrum analyzer system and on the transient digitizer illustrate typical results from the 1977 flight test program, and also indicate the way in which the two basic transient measurement techniques complement one another.

Figure 11 shows the record generated in the instrumentation associated with the analog tape recorder by lightning events starting at about 15:15:50 on 10 August 1977. In particular, the static field change associated with a flash occurring at 15:18:59 is evident in the record. The bottom trace in the record indicates that the digitizer was triggered by the electromagnetic transient associated with this flash. Other electromagnetic pulses were detected at this general time—mostly associated with nearby lightning flashes as evidenced by static field changes—but only the flash at 15:18:59 triggered the digitizer.

Data from the period starting at 15:18:59 are shown at a faster oscillograph writing rate in Figure 12. The higher time resolution of this record better reveals the structure associated with the development of the stroke. Note that only HF signals are evident in the record as the result of a combination of reasons. Although the E-antenna output

33

FIGURE 11   LIGHTNING – RELATED SPECTRUM ANALYZER RECORD

34
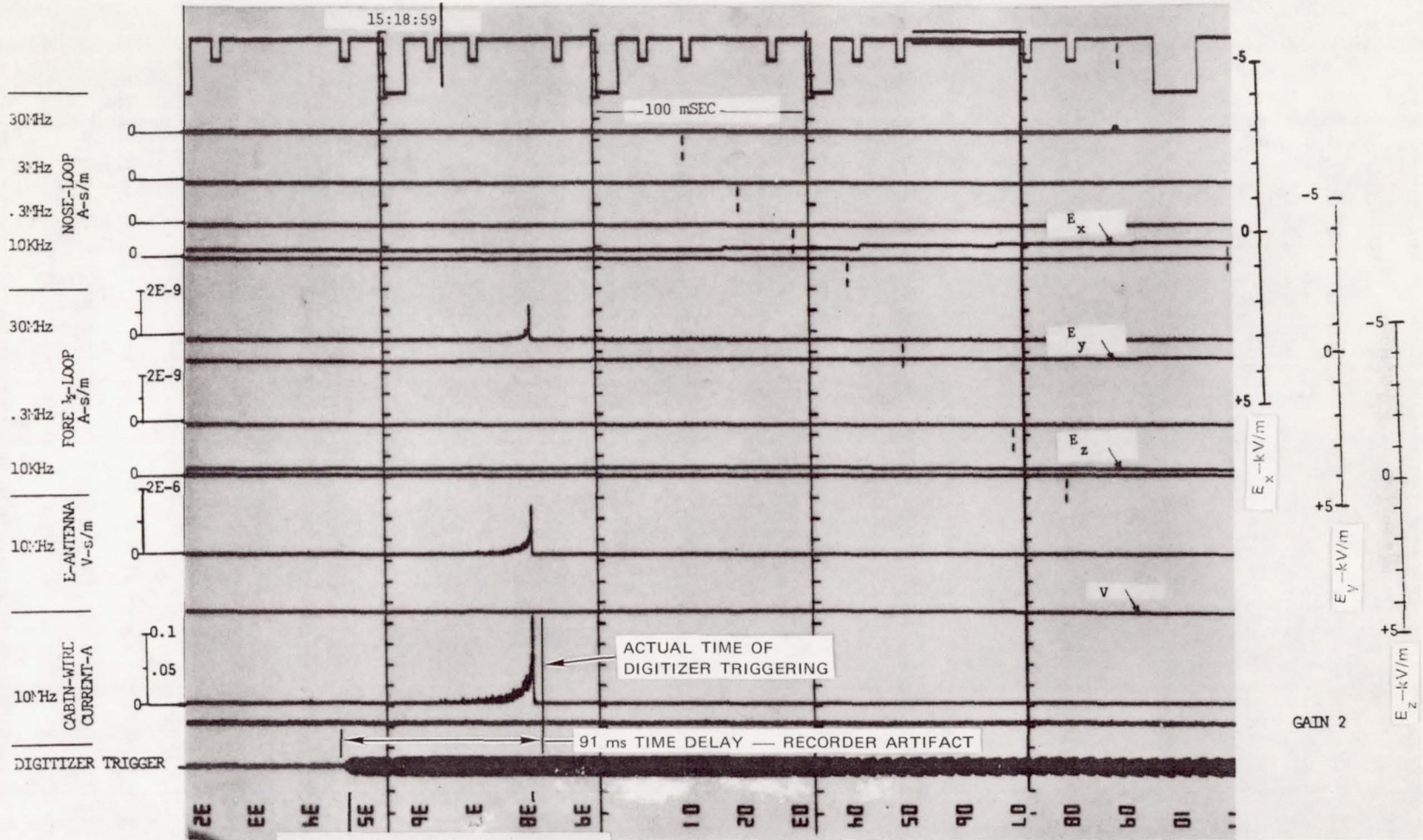
NOTE: Data from 10 August 1977.

FIGURE 12   HIGHER SPEED STRIPOUT OF LIGHTNING - RELATED SPECTRUM ANALYZER DATA

is directly proportional to E of the propagating transient field, only the 10 MHz channel was operating on the particular two-channel spectrum analyzer (No. 3) connected to the E antenna on this flight. The cabin wire short-circuit current is directly proportional to the fuselage current (see Appendix B of Reference 3). However, because the skin current is proportional to $\dot{E}$, the high frequencies will be accentuated. Accordingly, appreciable output from the cabin wire sensor was observed only on the 10 MHz channel. The forward fuselage skin current sensor was designed to respond to $\dot{J}$, so that the high-frequency portions of the transient were greatly accentuated.

An interesting feature of the noise pulse signals in Figure 12 is that perceptible noise starts at approximately 15:18:59.025 and increases intensity until it stops abruptly at 15:18:59.065--probably the time of the return stroke. This behavior is consistent with the observation that the HF components of the radiation associated with a lightning stroke are generated by the formative processes occurring prior to the return stroke.[12]

The apparent time delay between the beginning of the digitizer trigger pulse and the lightning event is an artifact of the tape recorder design. It results from the fact that the trigger pulse was recorded on the voice track, which uses the same head for recording and playback, whereas the data tracks are played back on separate heads located downstream of the record heads. Laboratory tests with the particular recorder used for data recording and readout indicated that this time delay is 91.6 ms at the tape speed used in generating Figure 12. Thus, the transient digitizer was actually triggered at about the time the formative processes of the stroke responsible for the high-frequency signals in the spectrum analyzer channels ended.

The digitizer record corresponding to the stroke of Figure 12 is shown in Figure 13. Although we cannot be sure, the rise time of the pulse (0.5 μs) and its general form are consistent with the transient signal generated by a cloud-to-ground lightning stroke. Note also that the peak field intensity of 75 V/m is suggestive of either a close (i.e., 6-8 km) intracloud flash or a rather more distant ($\sim$ 24 km)

36

cloud-to-ground flash. The static field change of ≈ 400 V/m is typical
of a cloud-to-ground flash 13 km from a ground measuring station.[13,14]
(See Appendix C.)

FILE NAME: F10AUG.29   MAXIMUM = .0746901 K U/M
TIME   15: 18: 59: 706   RISE TIME = .553851 U S
SENSOR: E FIELD (0DB)   DOM. FREQ. = 100 K HZ
SCALE: 377 U/M
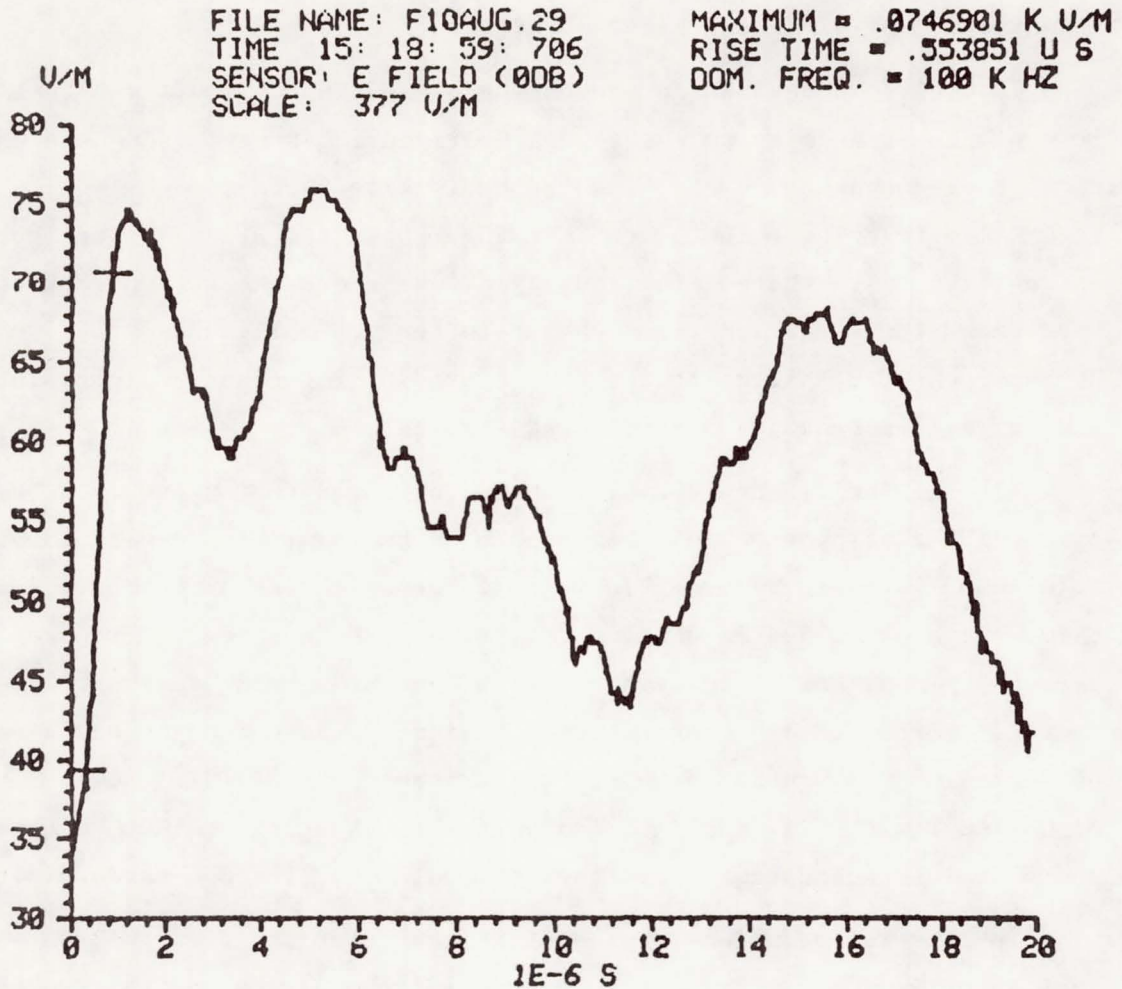
FIGURE 13   DIGITIZER RECORD CORRESPONDING TO STROKE OF LIGHTNING OF FIGURE 12

Further consideration of Figures 12 and 13 points out an important
shortcoming associated with the use of oscilloscope-like instruments to
record lightning signals. The digitizer was self-triggered by the ener-
getic low-frequency portion of the stroke, and missed the precursor
activity responsible for the generation of the HF noise in the spectrum
analyzer records. The sweep speed chosen also precluded recording the
overall (i.e., late time) pulse shape. Shedding light on the nature of

37

the high-frequency precursor activity was one of the objectives established for the digitizer system. Such information is needed to properly characterize signals coupling to the interior of aircraft through apertures. Overall pulse shape information would make possible some differentiation of different kinds of strikes.

If oscilloscope-like instruments are used in future flight tests, it would be wise to arrange a separate triggering system using the onset of high-frequency noise--such as the cabin wire current signal of Figure 12--to trigger the sweep. In Figure 12, the HF noise persisted in the cabin wire channel for roughly 40 ms before the return-current portion of the stroke. Triggering up to tens of milliseconds before the high-current part of the stroke should provide important insights into the early-time behavior of lightning strokes.

Alternatively, consideration should be given to the use of a basically different type of instrument such as the newly announced Biomation Model 6500 waveform recorder in which information is continuously fed through a storage system until a trigger occurs to stop the transfer process. In such a system, information generated prior to the trigger time is stored and can be read out at leisure. Some thought was given to employing a Biomation 8100 system for the tests of 1977; however the bandwidth limit of 25 MHz (Model 6500 has a bandwidth of 100 MHz) made the 8100 less appropriate than the Tektronix oscilloscope-based digitizer.

The Fourier transform of the digitizer record of Figure 13 is shown in Figure 14. This plot confirms the earlier observation that the high-amplitude lower-frequency signals associated with the return-current portion of the stroke completely dominate the transient digitizer record so that no spectral components are indicated above a frequency of 3.2 MHz. The transient digitizer flown on the Learjet was capable of recording frequencies to 500 MHz.

It is profitable to examine additional examples of records of the selected events generated by both the spectrum analyzer and the transient digitizer. One such record from 29 August 1977 is shown in Figure 15. Here, the transient digitizer was triggered at 16:21:17 by an event

38

1E-6 V/M
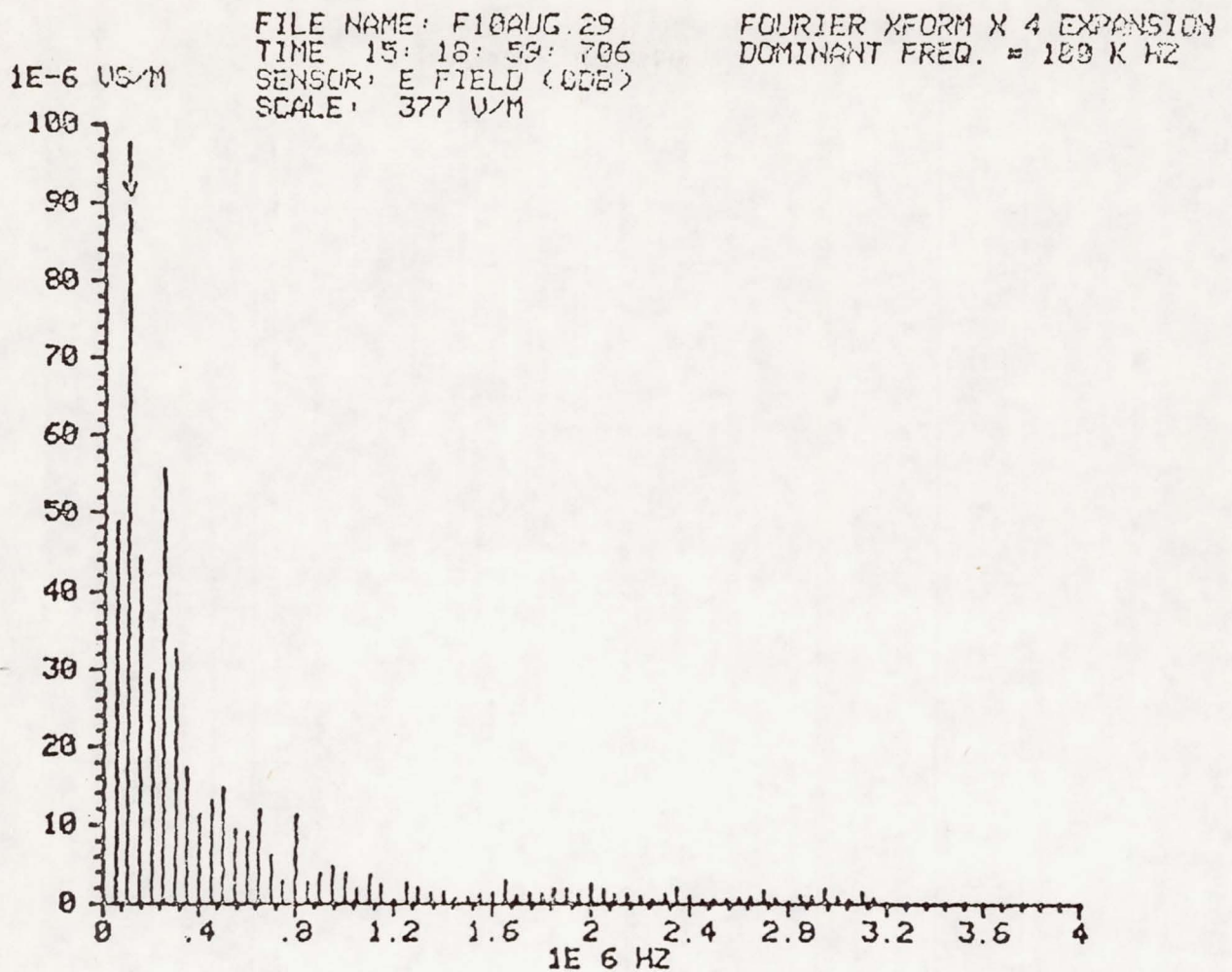
FIGURE 14   FOURIER TRANSFORM OF TRANSIENT DIGITIZER RECORD

that produced signals in the spectrum analyzer channels, but caused only a barely perceptible change in the electrostatic field. Thus, the signals were probably associated with a "far" lightning flash.

The high-time resolution oscillogram of the digitizer-triggering period is shown in Figure 16. It is interesting to note that the digitizer triggered approximately 6 ms after the precursor noise on the fuselage E-field antenna stopped.

The transient-digitizer time-domain record of the E-field antenna signal generated by the same event is shown in Figure 17. Although the digitizer apparently triggered substantially after the cessation of precursor noise, most of the pulse rise time is displayed. This result

39
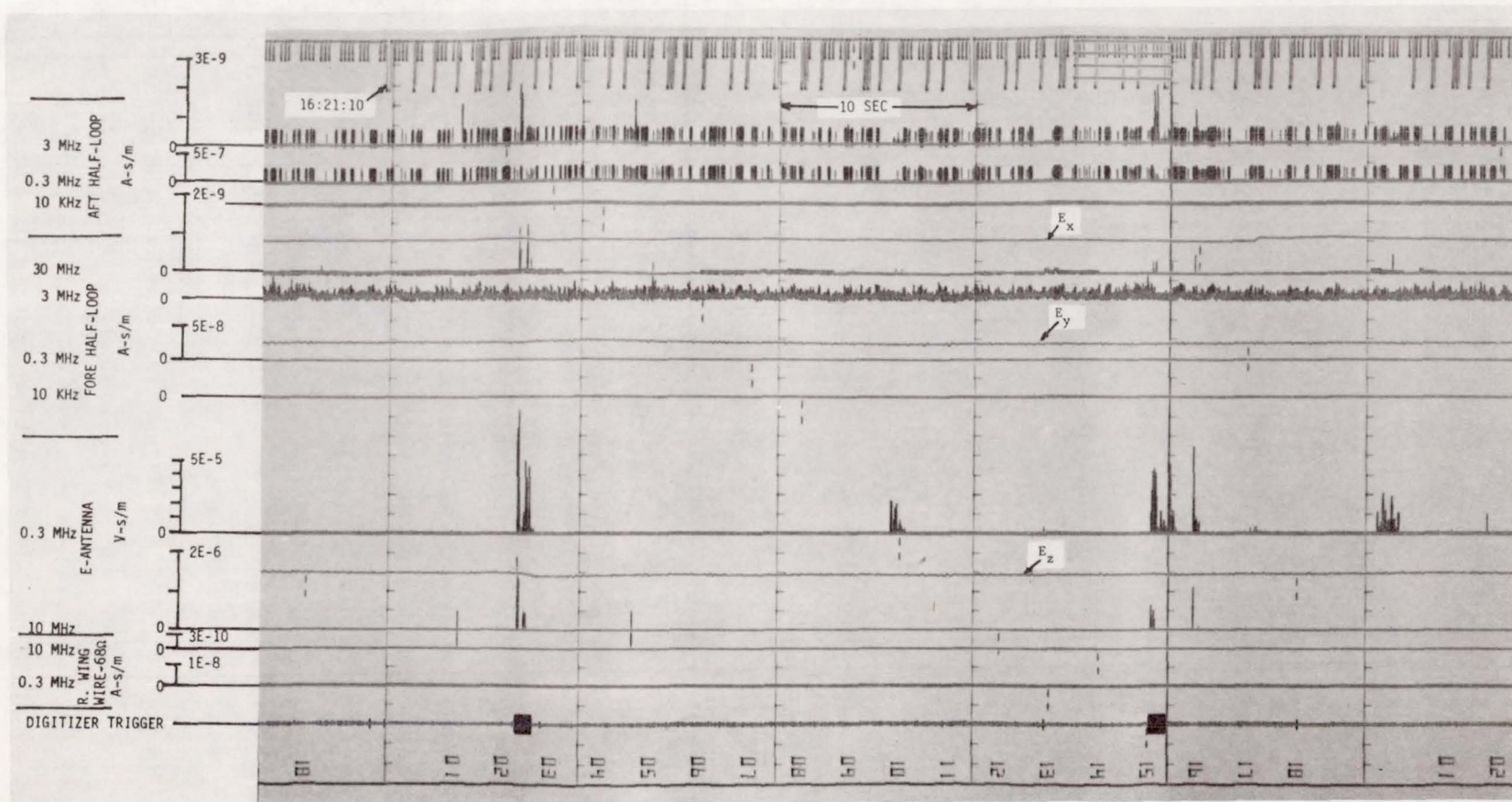
FIGURE 15 EVENT AT 16:21:17.87 AUGUST 29, 1977 CAPTURED BY SPECTRUM ANALYZER AND DIGITIZER

40
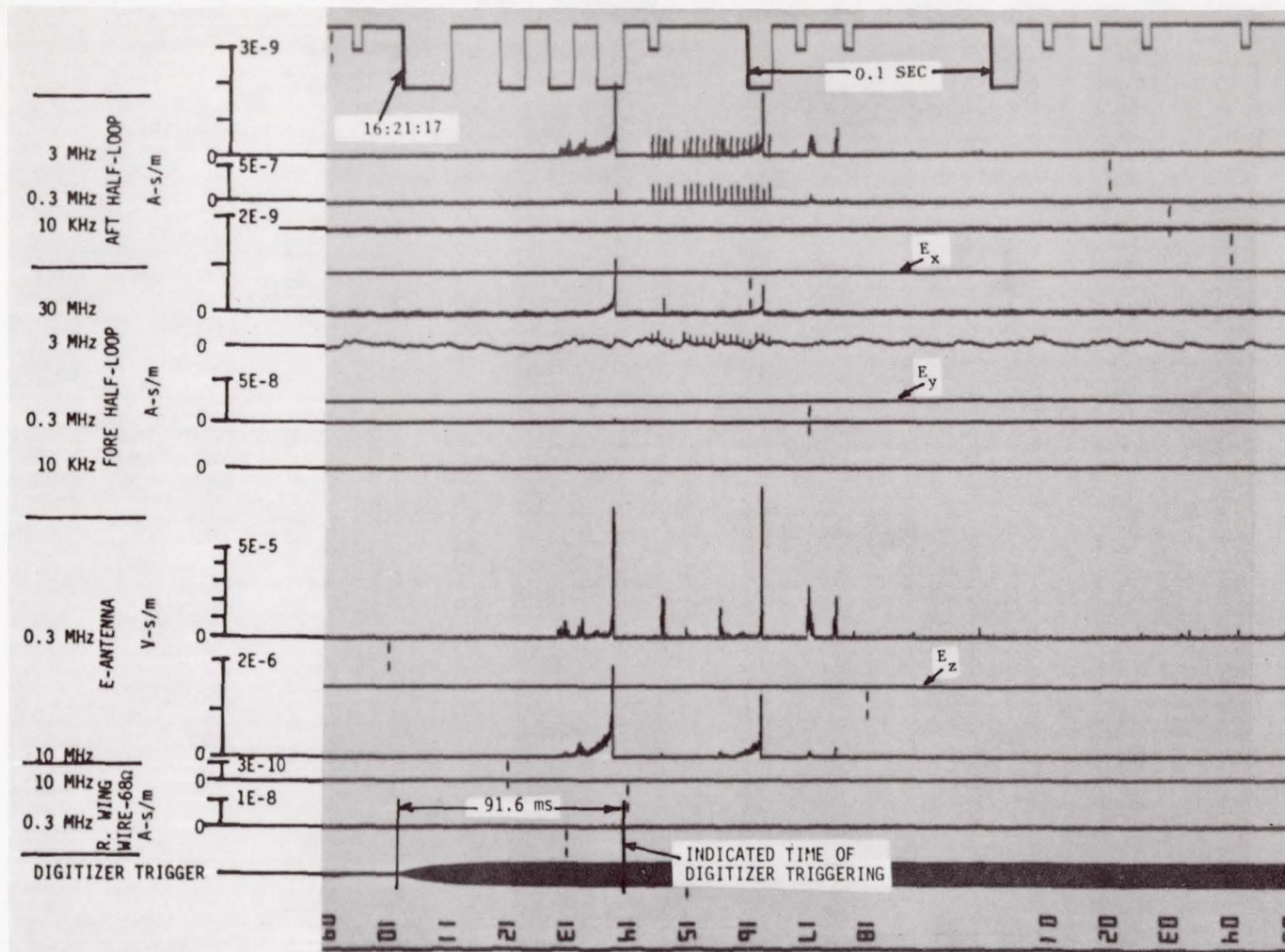
FIGURE 16   HIGHER TIME RESOLUTION OF EVENT 16:21:17.87, AUGUST 29, 1977

indicates that the precursor activity associated with a stroke can end substantially before the time of the return stroke. Such characteristics of lightning should be evaluated more carefully in future test programs.
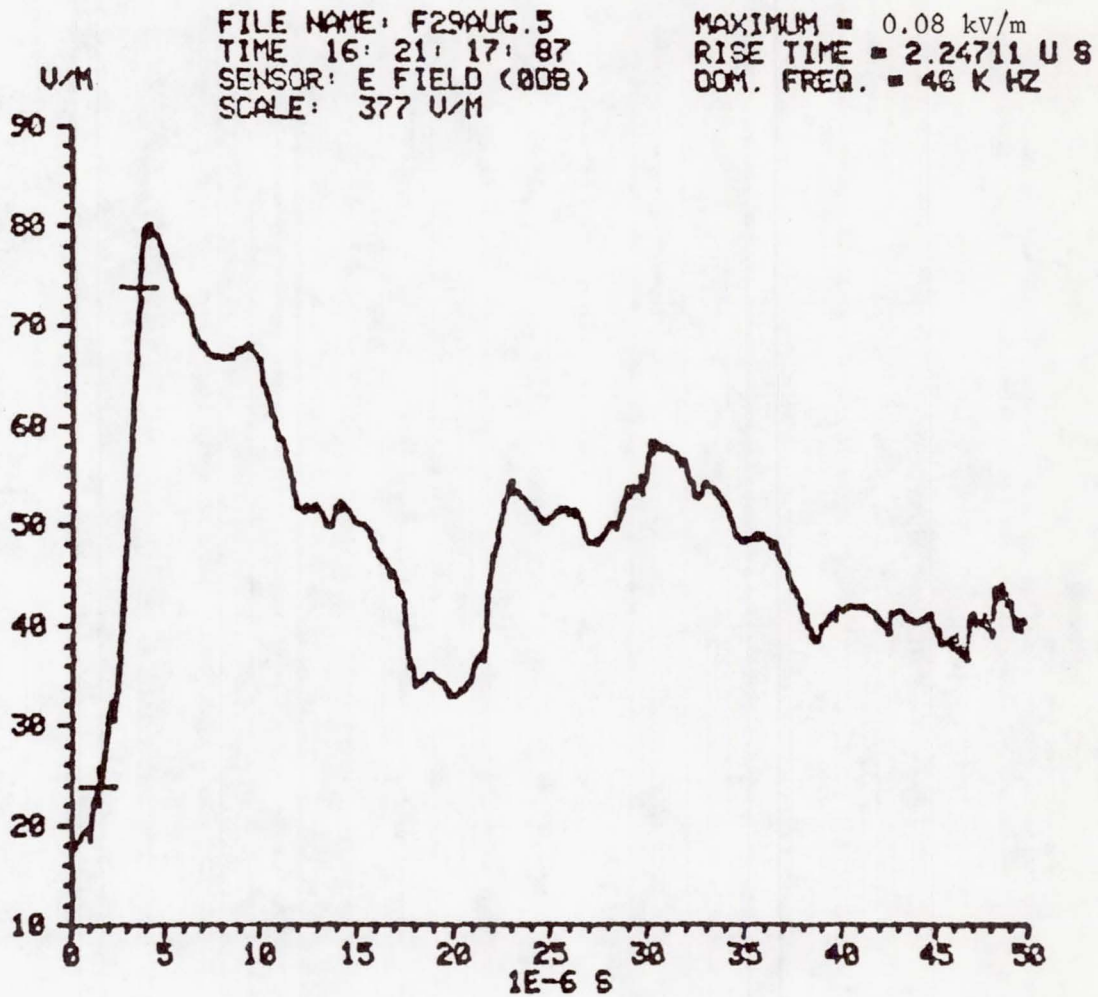
FIGURE 17   TRANSIENT DIGITIZER RECORD FOR 16:21:17.87, AUGUST 29, 1977

The Fourier transform of the digitizer waveform of Figure 17 is shown in Figure 18. It is interesting to compare the spectral-density magnitudes of Figure 18 with the maximum E-field-antenna spectral densities from the spectrum analyzer shown in the record of Figure 16. This comparison is made in Table 3. It is evident that the portion of the lightning signal recorded by the digitizer was not the one responsible for the high-frequency signals that couple into the aircraft interior.

42
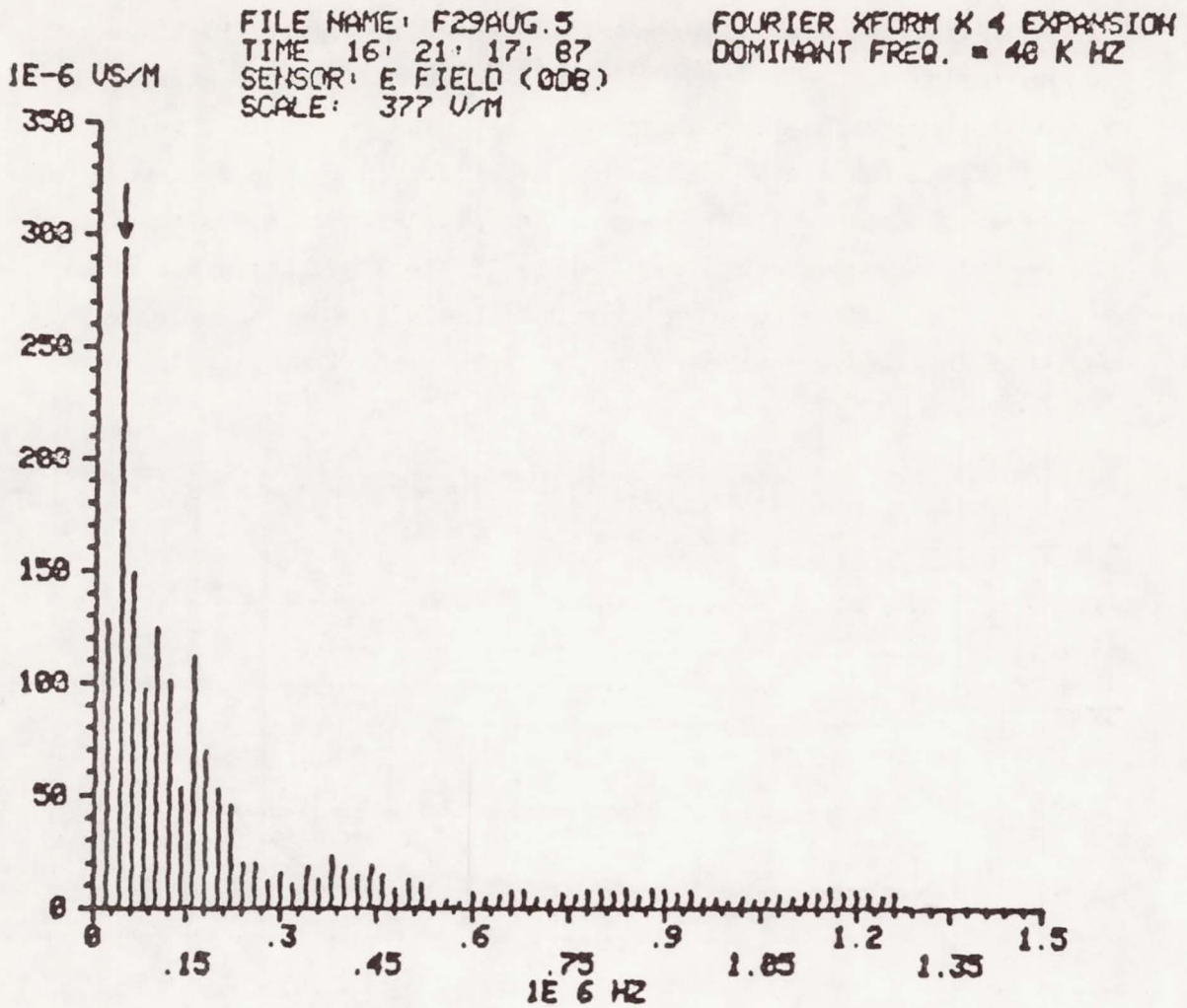
FIGURE 18   FOURIER TRANSFORM OF THE TRANSIENT DIGITIZER RECORD FOR
16:21:17.87, AUGUST 29, 1977

Table 3

COMPARISON OF SPECTRAL DATA GENERATED
BY TRANSIENT DIGITIZER AND SPECTRUM ANALYZER

	Spectral Density		
Frequency (MHz)	Digitizer $(10^{-6}$ V-s/m)	Spectrum Analyzer $(10^{-6}$ V-s/m)	Ratio of Spectrum Analyzer to Digitizer
0.3	16	> 1,600	> 100
10	< 1	> 30	> 30

43

Another event from 29 August 1977 (shown in Figure 19) illustrates the complexity of the electromagnetic signals that can be generated around an aircraft by lightning processes. The record in Figure 19 is associated with nearby lightning, as evidenced by the magnitude of the associated static field change. The pilot reported observation of "one of those long streaky ones." Very little RF activity was observed for tens of seconds before the event at 16:33:24, when a series of energetic RF pulses occurred. The "picket-fence-like" signals in the
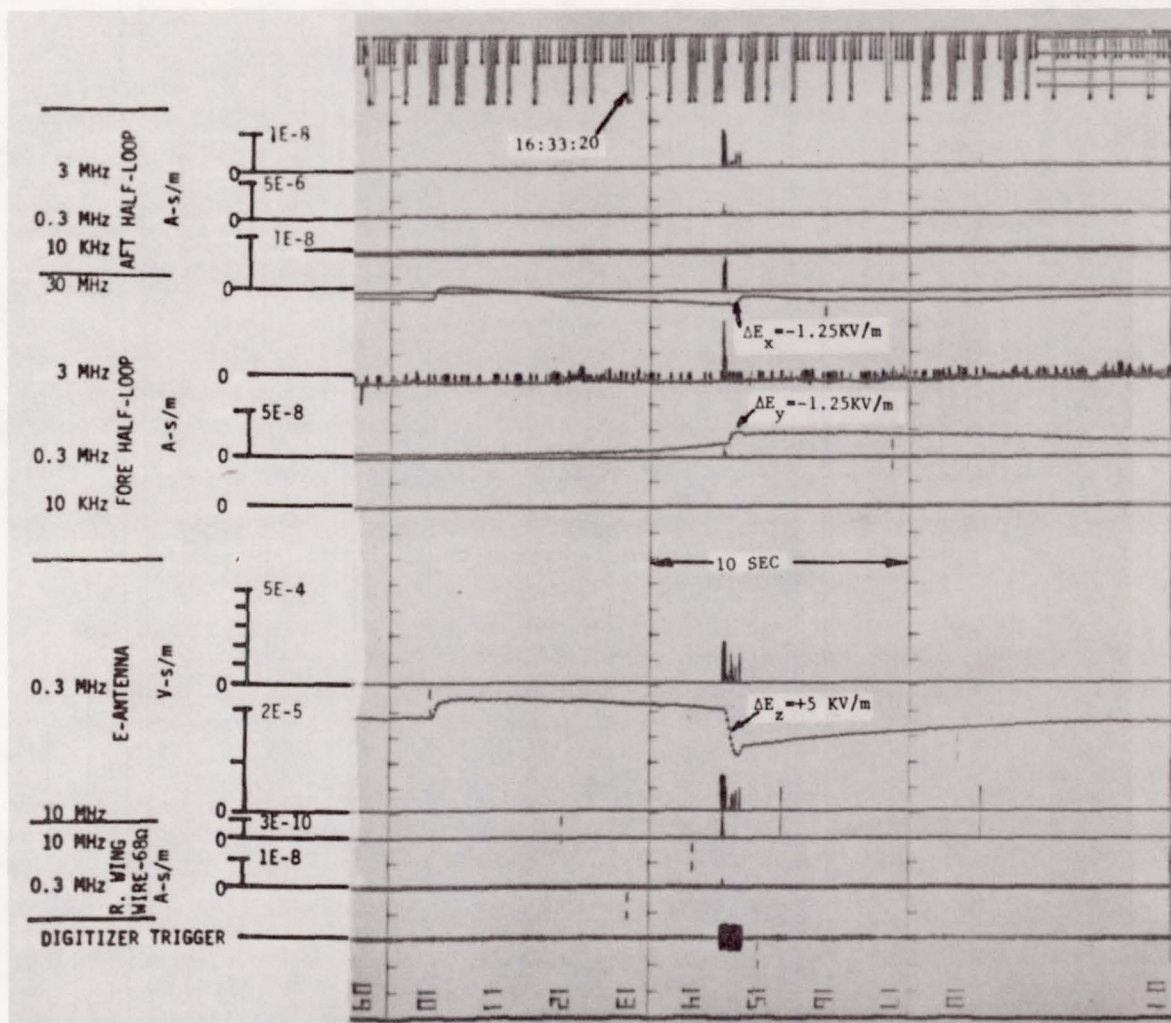
FIGURE 19   ELECTROMAGNETIC RECORD FROM "LONG STREAKY" FLASH AUGUST 29, 1977

aft-half-loop traces are the result of noise generated in the processing electronics and can be ignored.

Figure 20 shows the high-time resolution graph of this event. This time the transient digitizer did trigger when the spectrum analyzers indicated high-frequency signals. (We do not have the corresponding digitized time-domain event.) This record displays the many complex processes that occur in connection with a close lightning stroke, and shows that noise signal bursts can recur for periods up to a second or longer (see Figure 21). The individual bursts of RF noise also vary in their duration, ranging from tens of milliseconds to almost impulse-like times. The response of the right wing interior wire (shorted to the airframe at both ends) at 10 MHz and 0.3 MHz is interesting. Wing wire responses are not necessarily observed every time the driving signal (E field) is present. This is most likely because of differences between the antenna radiation patterns of the E-field antenna and the wire installed in the right wing. The pattern of the E-field antenna is approximately omnidirectional to vertically polarized signals, and the wing wire will respond only to those signals capable of exciting currents along the right wing. Unfortunately, at the time of the lightning event of Figures 19 to 21, the configuration of the instrumentation on the Learjet was such that wing skin current was not being recorded.

It is worth noting that on 18 August the right wing wires were re-routed to expose them to the opening between the flaps and the main part of the wing. This was done to increase their coupling to wing skin currents. (The wires in the left wing were routed entirely inside the skin.)

From Figure 20, it is evident that there is some difference even between the skin currents at the forward and aft fuselage skin current sensor locations. Some of the noise bursts that are prominent at the aft sensor do not produce a detectable signal at the forward sensor. This is possible because many modes of aircraft excitation are possible. The mode in which the fuselage is excited symmetrically would produce similar responses in both sensors. Other, asymmetrical, modes are possible in which the current flow, for example, is along the aft part

45
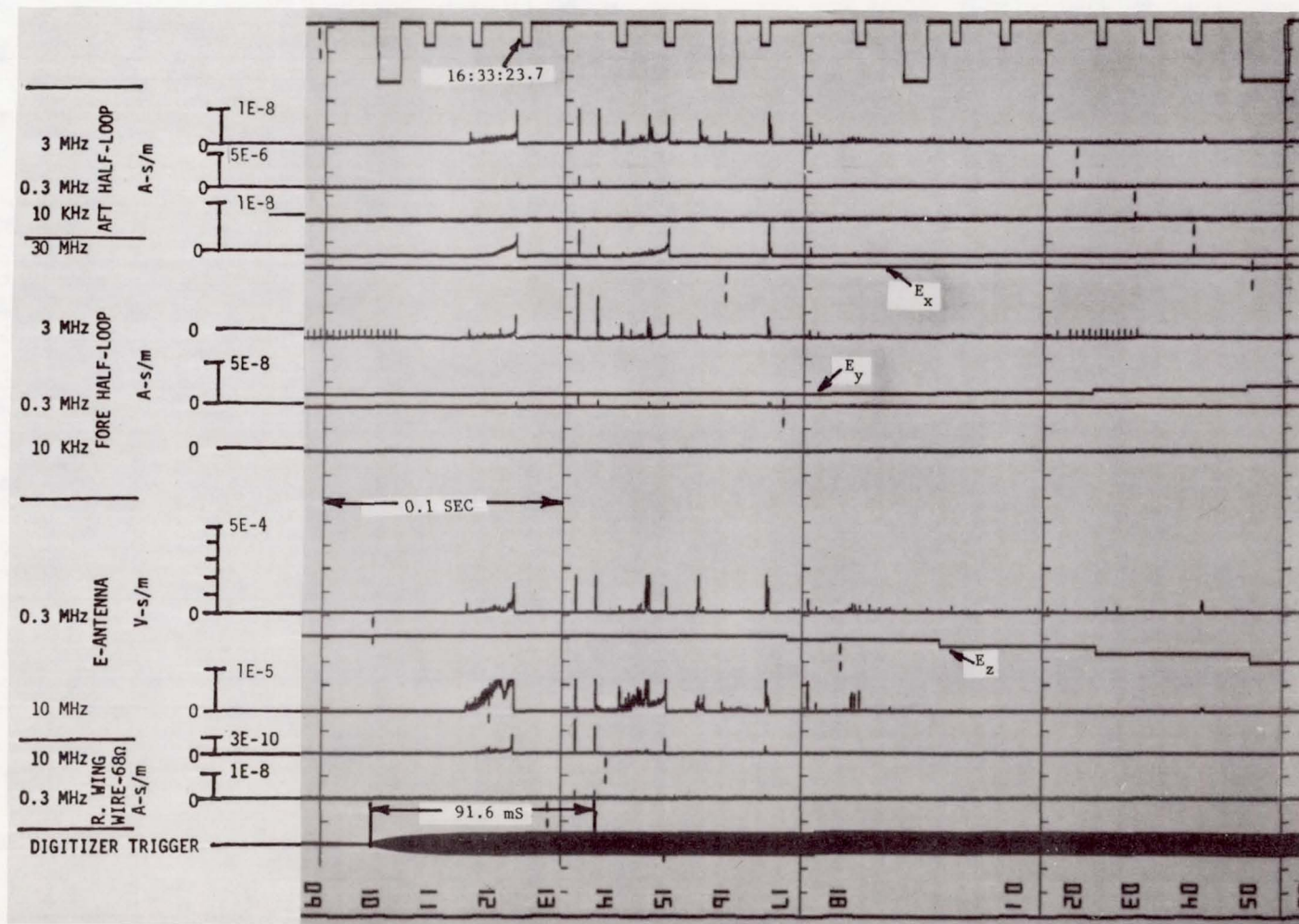
FIGURE 20   HIGH–TIME RESOLUTION RECORD OF "LONG STREAKY" FLASH STARTING AT
16:33:23.68, AUGUST 29, 1977
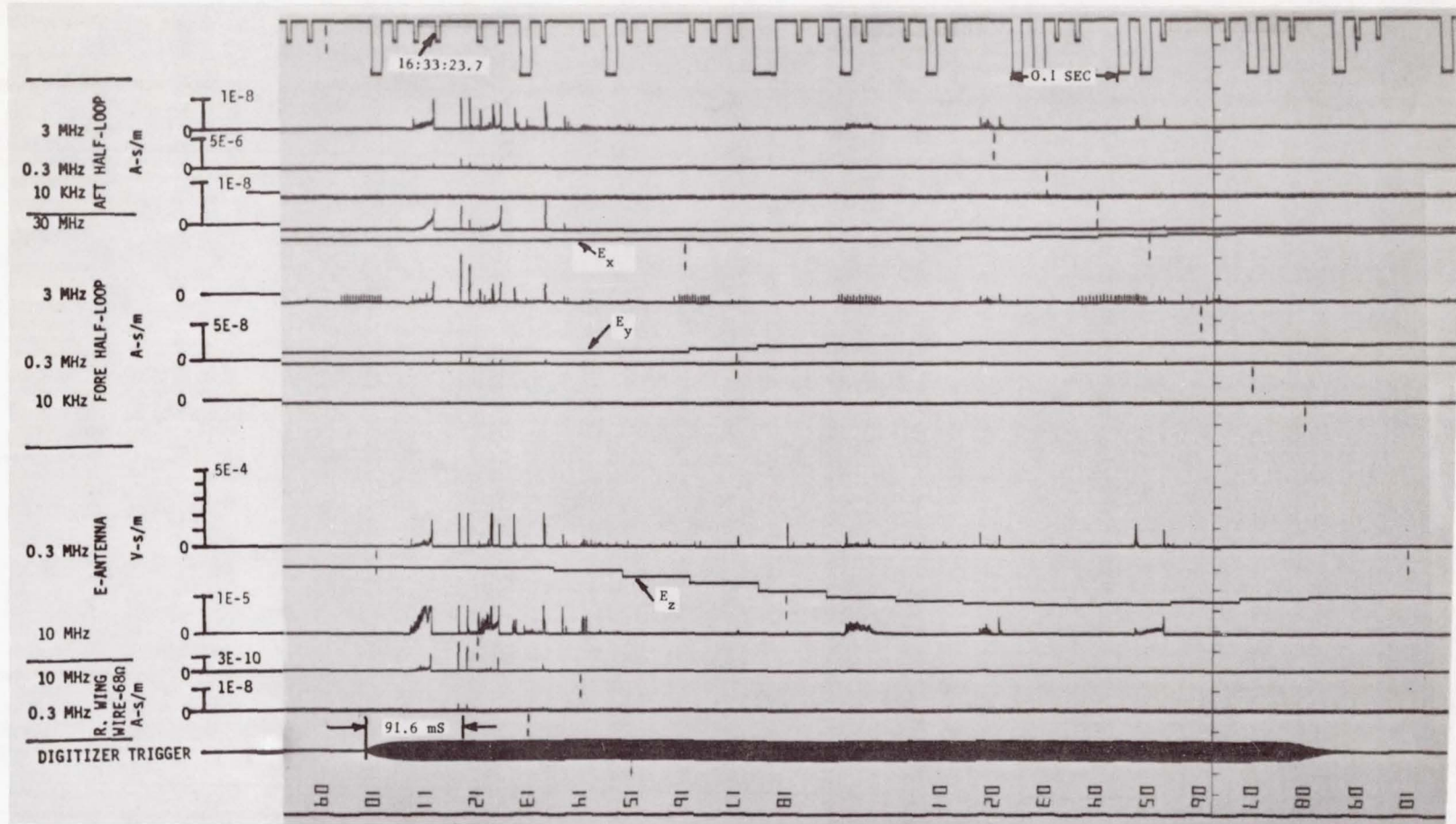
FIGURE 21   MEDIUM - TIME RESOLUTION RECORD OF "LONG STREAKY" FLASH STARTING AT
16:33:23.68, AUGUST 29, 1977

of the fuselage and on to the left wing. In this case, there would be response indicated in the E-antenna and the aft skin sensor, but no response in the forward fuselage skin current sensor or the right wing.

The record of another interesting lightning-associated event from 10 August 1977 is shown in Figure 22. At 15:15:22, there is a 2 kV/m step change in static field associated with a lightning flash that induced a pulse in the E-field antenna, thereby triggering the digitizer. The E-field antenna pulse shows up as a small signal on the 10 MHz spectrum analyzer channel used to monitor the E-field antenna. Also, it is evident that very little HF signal was generated in the cabin wire antenna.

The expanded time-scale record of this event is shown in Figure 23. This record shows none of the precursor activity characteristic of many of the lightning events shown earlier. Only a few high-frequency pulses are observed at about the time of digitizer triggering.

The transient digitizer record of this event is shown in Figure 24. The long rise time and the rounded time waveform confirm that the return-stroke transient would have very little HF content. Why this stroke did not have detectable precursor activity is not clear. Apparently, it is possible for some flashes to form without a great deal of preliminary streamer activity.

Lightning flashes accompanied by very little HF noise are not unusual because a similar flash occurred at 16:33:12.2 in Figure 19. The electrostatic field change associated with this flash is comparable to that which occurred with the highly noisy second flash in the record of Figure 19, but no detectable HF noise was generated by the first flash. Similarly, no HF noise was generated by the flash occurring at 14:03:58 in Figure 9.

The lack of precursor activity observed with some flashes is of great interest in connection with lightning location systems based on the detection of VHF signals from the flash.[15]
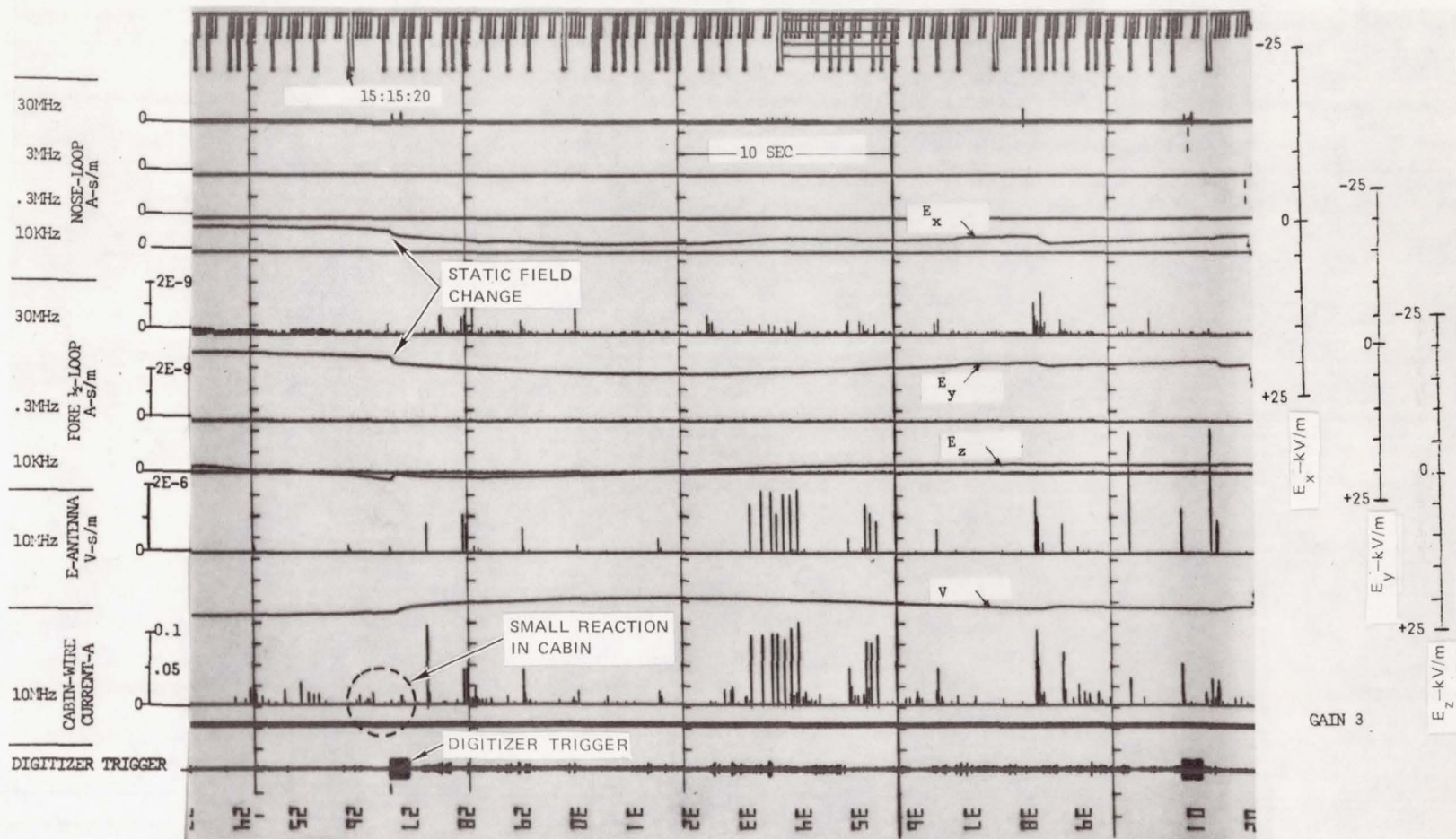
FIGURE 22   SPECTRUM ANALYZER RECORD OF LOW - FREQUENCY LIGHTNING EVENT
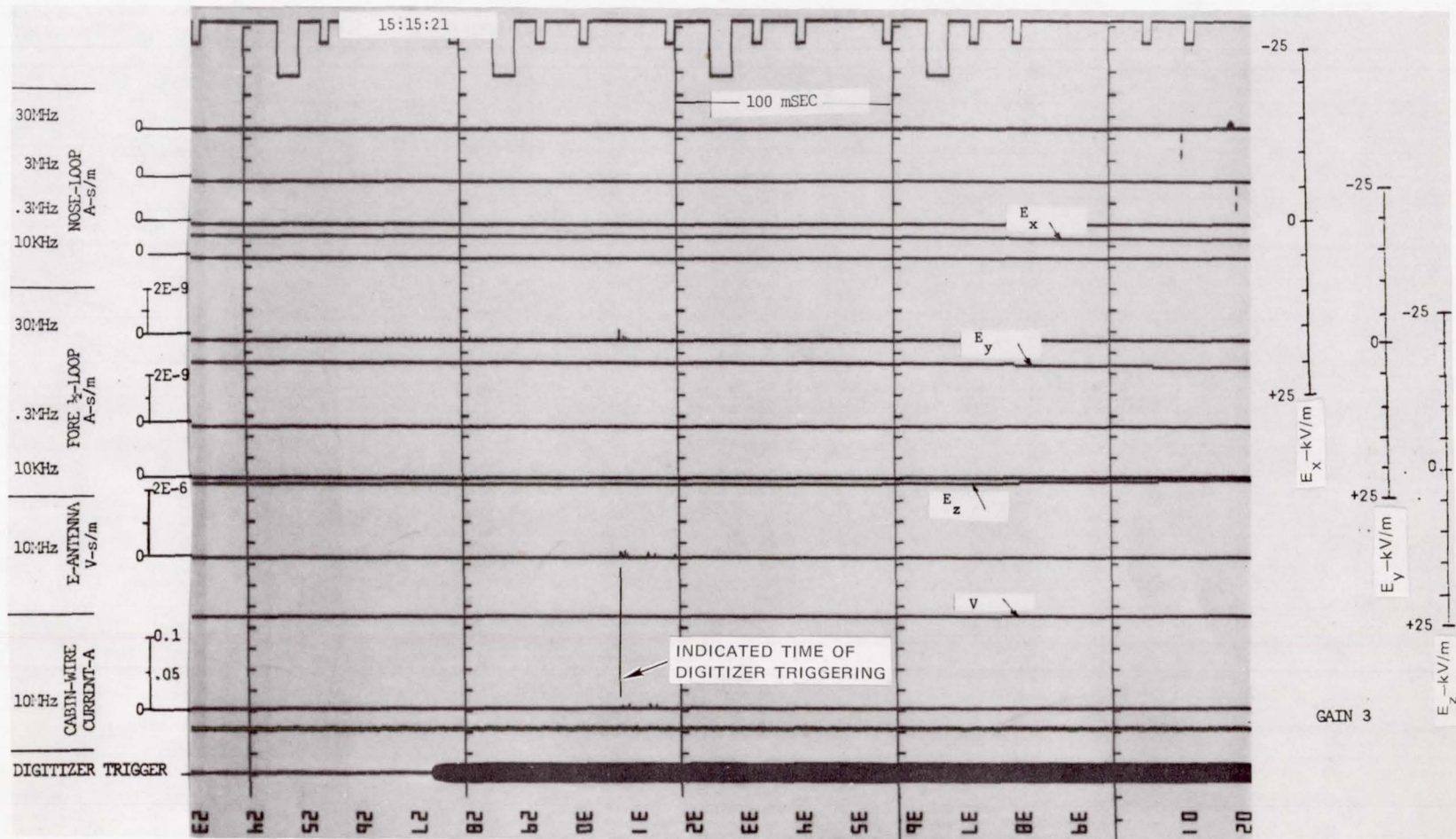
FIGURE 23   EXPANDED RECORD OF DATA FROM FIGURE 22

50

FILE NAME: F1OAUG.17   MAXIMUM = 9.65764E-03 K V/M
TIME 15: 15: 21: 697   RISE TIME = 4.6224 U S
SENSOR: E FIELD (ODB)   DOM. FREQ. = 50 K HZ
SCALE: 377 V/M
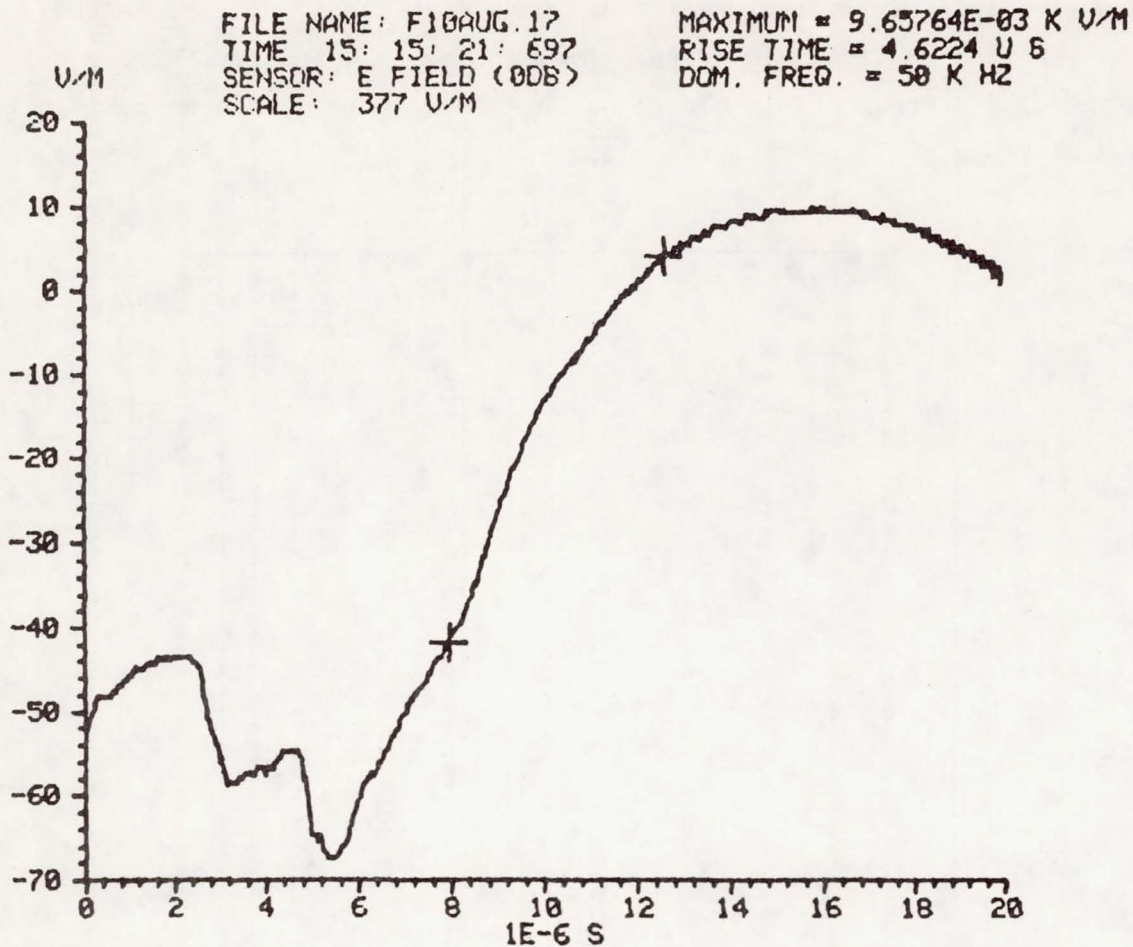
FIGURE 24 TRANSIENT DIGITIZER RECORD OF LOW-FREQUENCY LIGHTNING EVENT

Data Summary

Using records of the sort presented thus far in Section IV, tabu-
lations and graphs were prepared in an effort to generalize some of
the results of the flight tests. Figure 25 shows a plot of the radiated
electric field intensity at 10 MHz versus the associated change in total
electrostatic field. This plot is of interest because the static field
change is a reasonable indicator of the distance to the flash according
to the following argument. As is indicated in Appendix C, the static
electric field change associated with a lightning flash falls off as the
cube of the distance.[13] Accordingly, uncertainties in field magnitude

stemming from uncertainties regarding source magnitude are swamped out by the rapid decay of the static term with distance.[14] (To place the field charge magnitudes in perspective, it may be noted from Figure C-1 that a 1 kV/m static field change on the ground corresponds approximately to a distance of 10 km from the storm.)
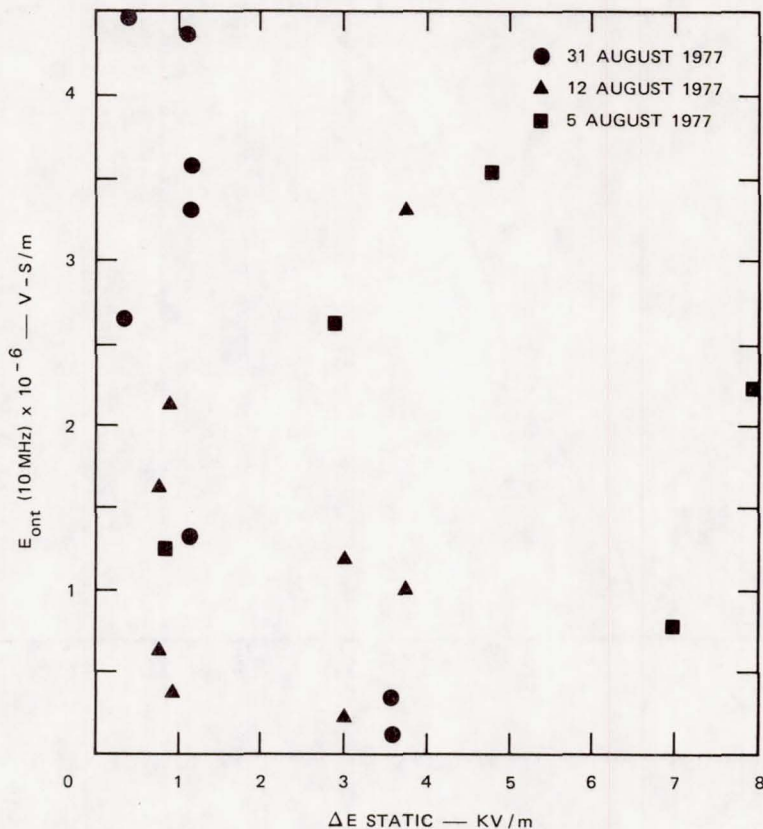
FIGURE 25   STATIC FIELD CHANGE VERSUS E - ANTENNA SPECTRAL DENSITY
AT f_o = 10 MHz

It is evident from Figure 25 that for any given static field change (distance from the cell), there is a great variation in the 10 MHz signal level. This result is consistent with the postulate that the HF noise generated by a lightning flash occurs during the period of streamer and leader formation prior to the return stroke.* The level of this activity is not necessarily related to the total charge ultimately neutralized.

---

*See the discussion of Figure 12 earlier in this section.

52

(Some of the flashes observed appear to produce virtually no HF signal.) In addition, the location of the stroke with respect to the aircraft and the orientation of the stroke current channel affect the amplitude of the 10 MHz signal.

Accordingly, the data of Figure 25 should be taken simply as being an example of the 10 MHz signal environment encountered by an aircraft operating 10 km and closer to an active thunderstorm cell. Because so few data points were available for $\Delta E > 1$ kV/m, it is probably not prudent to assume that the plotted data are truly representative of the 10 MHz signals closer than 10 km from the cell.

The data of Figure 26 indicate peak cabin wire current signals as a function of E-field antenna signal. The data are from the flight of
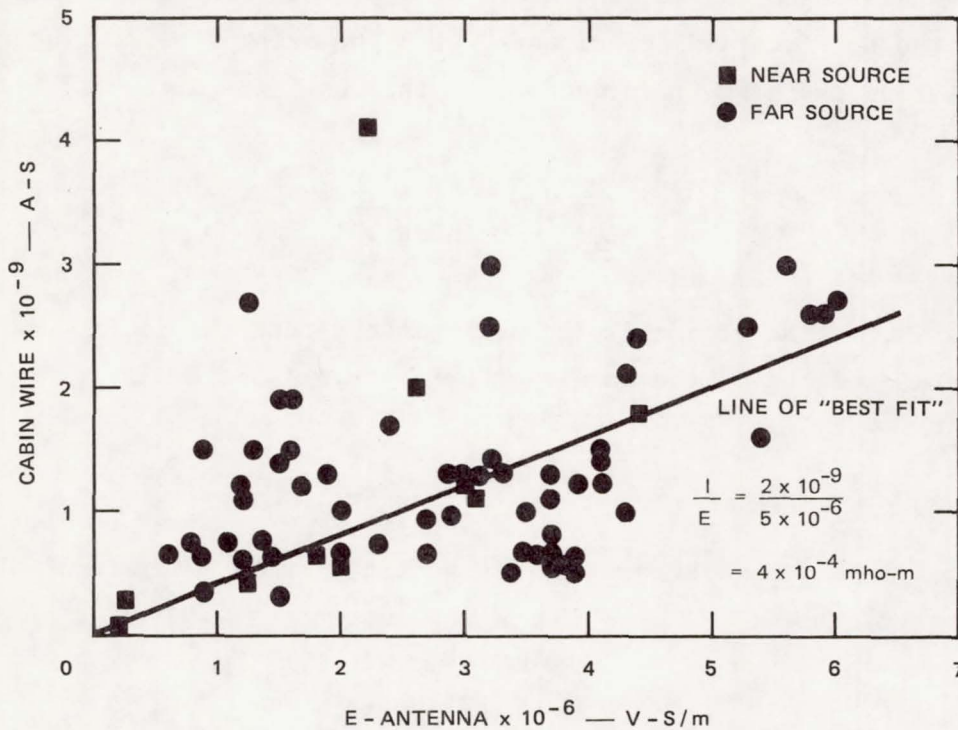
FIGURE 26   INDUCED CABIN WIRE CURRENT SPECTRAL DENSITY VERSUS E - ANTENNA FIELD SPECTRAL DENSITY AT 10 MHz

53

10 August 1977 and indicate cabin wire responses from both near and far sources. The wide spread in the data stems from the fact that the E-field antenna responds primarily to the E_z component of field whereas the cabin wire is driven by currents along the fuselage that couple most strongly to the E_y component of electric field. Thus, it is possible to have substantial fuselage excitation with low E-field antenna readings or to have very little excitation of fuselage current with a high E_z.

It is interesting to calculate a transfer function for cabin wire current in terms of the E-field antenna readings. To do this, let us take the broken line in Figure 26 as being the line of "best fit" for the plotted data. The slope of the line gives the transfer admittance

$$\frac{I}{E} = 4 \times 10^{-4} \text{ mho } -\text{m} \quad . \tag{10}$$

From Reference 16, we find that for a cylinder the length and diameter of the Learjet fuselage situated with the axis of the cylinder along the direction of the E-field vector, E, the fuselage current I_{fus} is given by

$$I_{fus} = 0.132 \, E \quad . \tag{11}$$

In Appendix B of Reference 3, it was estimated that the cabin wire current I_w was related to the fuselage current by

$$I_w = 6.44 \times 10^{-4} \, I_{fus} \quad . \tag{12}$$

Combining these two relationships, we obtain a crude estimate of the transfer admittance:

$$\frac{I_w}{E} = 6.44 \times 10^{-4} \, (0.132)$$

$$\simeq 10^{-4} \text{ mho } -\text{m} \quad . \tag{13}$$

Thus, coupling to the cabin wire determined from the measured data of Figure 26 is only slightly higher than that predicted by the crude analysis.

54

Coupling of signals to a wire on the interior of the right wing is shown in Figure 27. On 12 August 1977, spectrum analyzer No. 4 was used to monitor the signals induced in the 68-ohm-terminated wire in the right wing. (For this flight, the sensor wire was run entirely on the interior of the wing. Later, on August 18, the wires in the right wing were rerouted to pass through the region between the flaps and the main part of the wing to increase their coupling to wing skin currents--see the data of Figure 21.) Although the data in Figure 27 are quite sparse, with the exception of two high-amplitude points, the currents are approximately the same as those induced in the cabin wire of Figure 26.
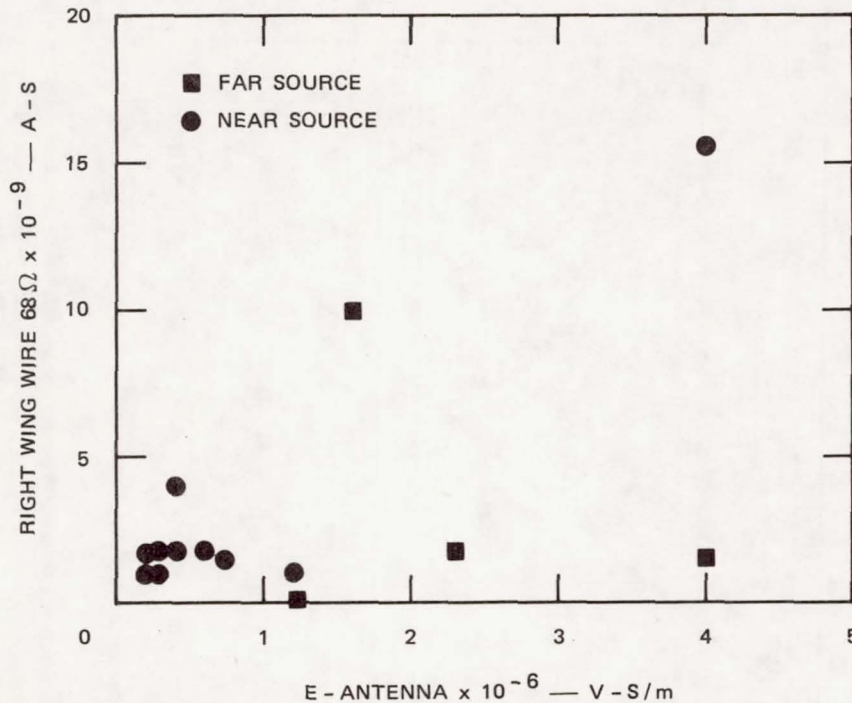
NOTE: Data from flight of 12 August 1977.

FIGURE 27   RIGHT WING WIRE CURRENT SPECTRAL DENSITY VERSUS E - ANTENNA FIELD SPECTRAL DENSITY AT 10 MHz

55

This result is reasonable because the portion of the wire run in the wing may be expected to have relatively little current induced in it as a result of the wing having fewer large apertures than the fuselage. On the other hand, much of the "wing wire" actually ran through the cabin to the current sensor at the top of the instrumentation rack. Because the length of the run inside the cabin was approximately the same as that of the "cabin wire" sensor, it is not surprising that the current magnitudes are similar.

The relationship between right wing skin current density and E-antenna signal is shown in Figure 28 for the flight of 9 August 1977. There is substantial spread in the data largely because the E-antenna responds primarily to the E_z component of electric field whereas the wing skin current couples most strongly to the E_x component of electric

$J/E = 0.00825$

RIGHT WING $J \times 10^{-8}$ — A − S/m

E − ANTENNA $\times 10^{-6}$ — V − S/m
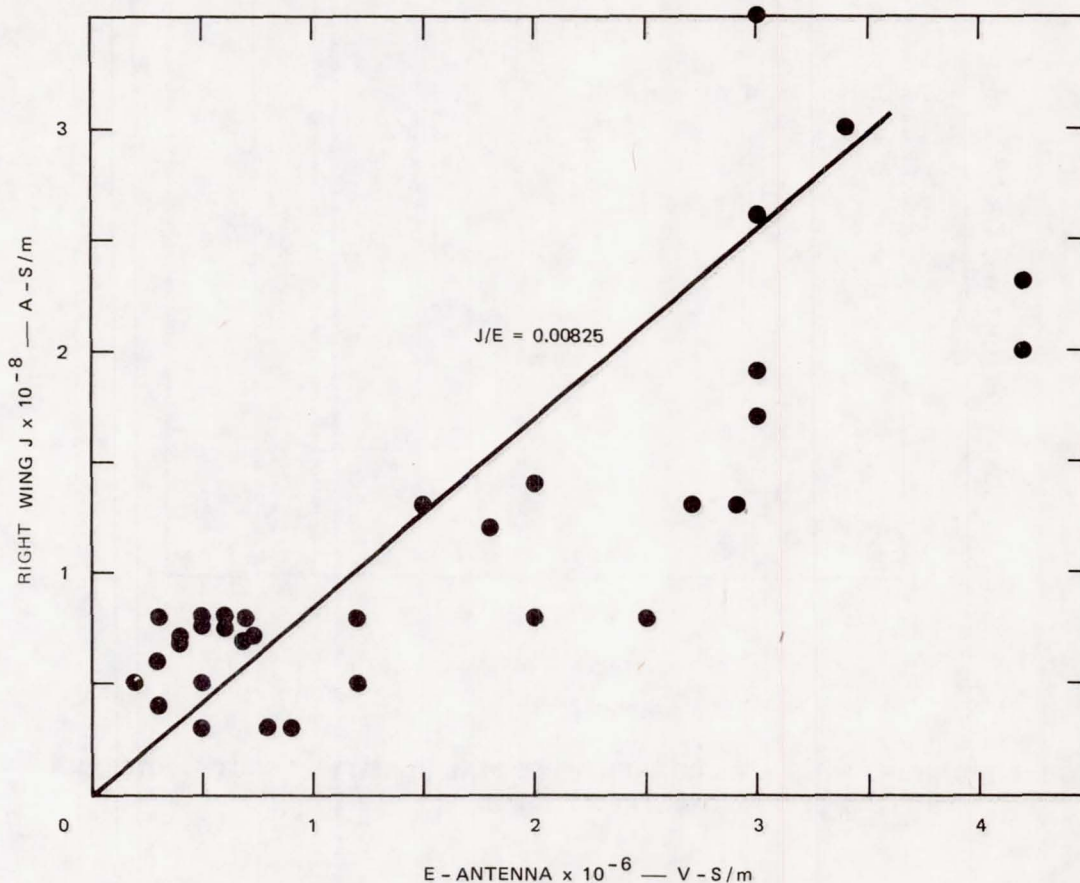
NOTE: Data from flight of 9 August 1977.

FIGURE 28   RIGHT WING SKIN CURRENT SPECTRAL DENSITY VERSUS E − ANTENNA FIELD SPECTRAL DENSITY AT 10 MHz

Thus, it is possible to have substantial wing current excitation with low E-antenna reading or to have little excitation of wing current with a high E_z.

In spite of the large spread in the data, it is instructive to compare the general relationship of Figure 28 with the results of a crude analysis. Let us argue that, to a first approximation, the currents induced at the root of the wing by a field E along the wing is the same as the current induced at the midpoint of the fuselage by a field E along the fuselage. It was indicated earlier in Equation (11) reproduced here that this relationship is

$$I = 0.132 \ E \quad .$$

Because the skin current sensor is slightly over half way to the wing tip, the current at the sensor location would be expected to be less than half that at the wing root were it not for the fact that the presence of the fuel tank at the tip produces some end loading and increases the current. Thus, we will assume that the wing current at the sensor location is half the current at the wing root, or

$$I_{wing \ sensor} = 0.066 \ E \quad . \tag{14}$$

To calculate the current density, J, at the current sensor location, we note that the circumference of the wing at the sensor location is 2X chord, or 4 meters. Thus, the average current density at this wing station is given by

$$J_{avg} \cong \frac{I_{wing \ sensor}}{4}$$

$$\cong \frac{0.066 \ E}{4}$$

$$= 0.0165 \ E \quad . \tag{15}$$

However, we observe that the current density is not evenly distributed over the wing. It is highest near the edges of the wing and lowest in the middle. Let us assume that the current density at the sensor location is half the average J or

$$J_{\text{wing sensor}} = 0.0083 \text{ E} \quad . \tag{16}$$

The line representing this calculated relationship between J and E is plotted in Figure 28. The agreement between this approximate analysis and the measured data is remarkably good.

Data from the flight of 17 August 1977 comparing nose loop H-fields and E-antenna E fields at a frequency of 0.3 MHz are shown in Figure 29. Again, it is evident that the data are quite scattered because there may be substantial variation from flash to flash in the position of the lightning with respect to the aircraft and in the orientation of the channel. These differences between the flashes affect in different ways the field
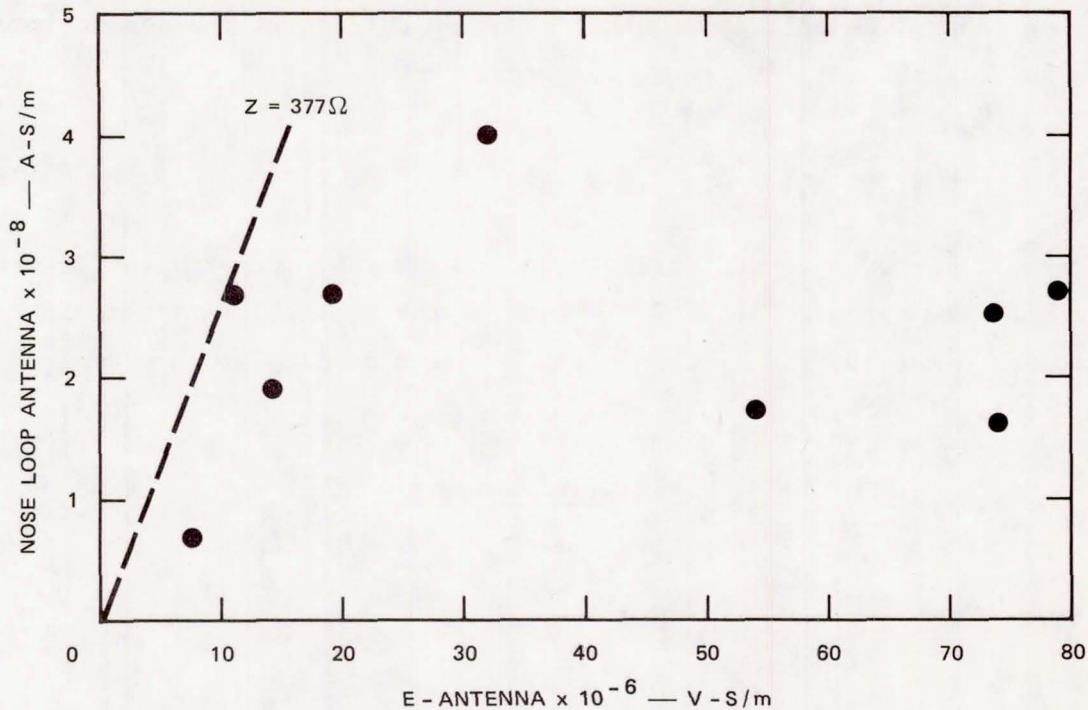
NOTE: Data from flight of 17 August 1977.

FIGURE 29   NOSE - LOOP - ANTENNA FIELD SPECTRAL DENSITY VERSUS E - ANTENNA FIELD SPECTRAL DENSITY AT 0.3 MHz

58

components responsible for generating nose loop signals and those components responsible for E-antenna response.

At the right of Figure 29 is a line representing Z_o = E/H = 377 ohm, which relates the E and H fields in a plane, propagating wave. It is evident that E/H measured for all of the strokes in the figure is greater than 377 ohm. This result may stem from several causes. First, in the near field of an electric dipole, the electric field dominates and E/H > 377 ohm. Thus, if the aircraft is in close proximity to the stroke channel, we can expect this result. Second, although neither the E-antenna nor the nose loop responds to the total field at its location, the E-antenna has an omniazimuthal response to E_z. The nose loop responds primarily to H_y and has a null in the forward direction, and is insensitive to the H-field component generated by a horizontal discharge channel along the fuselage of the aircraft. Because there are several ways in which the nose loop can be decoupled from the H-field generated by the stroke, it is not surprising that in the limited sampling of Figure 29, the nose loop outputs are all lower than would be predicted by the simple application of the relationship $H = E/Z_o$. Finally, the apparent H-fields indicated by the loop may be too small because the loop was calibrated for free space, but it is used near a conducting bulkhead.

Page intentionally left blank

V CONCLUSIONS

The 1977 Learjet program produced results of great significance to the understanding of lightning-induced noise in avionics systems. Perhaps of greatest importance is the fact that the precursor activity associated with a stroke often produces high-frequency noise of greater duration and amplitude than does the main return stroke.

This phenomenon is of importance because the "standard stroke" currently widely used for noise calculations does not include components associated with this precursor activity and is therefore not adequate, in many cases, for accurate noise calculations and predictions. For example, the spectrum of the two-exponential return stroke current model decreases as f^{-2} at frequencies above about 200 kHz, whereas the observed high-frequency spectrum of the fields only decreases as f^{-1} to well above 20 MHz (see Reference 12). These larger high-frequency fields observed at large distances (> 10 km) are undoubtedly produced by the precursor activity observed at closer range in the 1977 Learjet program.

In many cases, it was found that this precursor activity and its associated noise ended at the beginning of, or perhaps several milliseconds before, the time of the return stroke. This appears to be consistent with the "quenching" effect of the return stroke described by Cianos, Oetzel and Pierce.[12]

Also interesting is the fact that the precursor activity was not observed with some strokes. The reason for the absence of the precursor is not understood, but it may have important implications on lightning detection and warning systems that rely on the high-frequency signals from thunder storms.[15]

In addition to confirming the existence of the high-frequency precursor noise source, the results of the 1977 program indicated that the induced high-frequency noise on internal wires is often of greater

61

amplitude and of longer duration than that produced by the main return stroke. Because high-frequency external noise couples most readily through aircraft apertures, the precursor activity is probably the major source of noise induced in internal aircraft systems by nearby lightning activity.

The noise signal levels measured on the interior of the Learjet may be taken as typical of those expected on an all-metal aircraft. Incorporating more electromagnetic apertures in the aircraft will raise the levels of the induced currents. Precise signal levels and waveforms that are determined by resonances of the airframe and internal wiring will also vary from aircraft to aircraft.

The 1977 test program also provided useful insights regarding instrumentation appropriate for the airborne studies of lightning and its effects on aircraft. The concept of providing sensors to follow the lightning electromagnetic signal from propagating field to airframe current to currents on interior wiring proved to be sound in that it allows the coupling process to be separated into natural steps. The precise choice of sensors, sensitivities, and preamplifiers for the 1977 program stemmed from a variety of constraints, and would probably be modified somewhat in future studies.

The concept of using a continuously operating spectrum analyzer in conjunction with a periodically triggered transient digitizer also proved to be sound in that one measurement technique complemented the other. In general, the digitizer appears to have recorded the signal generated by the return stroke, but did not record the precursor activity preceding the main stroke. This stemmed from the fact that the broad-band oscilloscope input on the digitizer system may have been triggered on the energetic, low-frequency portion of the lightning signal.

To investigate the nature of the precursor activity, it is recommended that provision be made either to trigger the digitizer from a source tuned to HF (for sample, 10-30 MHz) or to use a storage type of transient measurement system such as the Biomation 8100, which allows the readout of data generated and stored before the trigger.

Because the nature of the precursor activity is such that many HF pulses can occur tens of milliseconds before the main stroke, large memory sizes would be needed to continuously digitize both the precursor events and the main stroke. A promising approach would be to use two digitizer channels to record data from the same sensor with provisions to trigger both sweeps simultaneously from the same high-frequency source. One channel with a high-speed sweep would define the precursor activity while the second channel with low-speed sweep would display the overall stroke.

In view of the gaps still remaining in our understanding of the precursor phenomena, together with the fact that much of the basic Learjet instrumentation is still intact, it appears appropriate to continue to fly the Learjet system (modified appropriately) to acquire the required data. The amount of instrumentation carried on the aircraft should be reduced sufficiently that packaging and installation would not constitute a major fraction of the effort. The choice of a transient measuring system and its triggering arrangements should receive careful attention to make certain that critical questions are addressed properly.

The Florida area in the summer appears to be a good choice for the flight test site. Substantial planning and coordination with local agencies should precede the actual tests. In particular, supporting data from the KSC lightning detection and ranging (LDAR) system might be of substantial use. Because the LDAR depends upon VHF time-of-arrival measurements for its operation, it is most responsive to the precursor activity associated with lightning.[15]

Page intentionally left blank

Appendix A

LEAKAGE THROUGH SHORT CYLINDRICAL CABLE SHIELDS[*]

Page intentionally left blank

Appendix A

LEAKAGE THROUGH SHORT CYLINDRICAL CABLE SHIELDS

General

In connection with the study at SRI of electromagnetic leakage
through cable shields, data were obtained that are relevant to the prob-
lem of coupling of lightning-induced signals to the interior of aircraft.
The results are very graphic in demonstrating the differences between
the signals produced by diffusion through the skin and those produced
by aperture coupling. In particular, the results demonstrate the impor-
tance of considering the high frequency processes associated with actual
lightning strokes or those generated by the simulator when aperture
coupling is involved.

Experimental Setup

The experimental setup used in the laboratory measurements of elec-
tromagnetic leakage into shielded cables is shown in Figure A-1. A
current pulse is induced on the outside of the outer cable shield by
charging a 2-μF capacitor until a spark-gap switch fires and discharges
the capacitor through the cable shield. The discharge current returns
to the capacitor through an aluminum tube concentric with the cable. A
$CuSO_4$ resistor in series with the capacitor has a value approximately
equal to the characteristic impedance of the transmission line formed by
the test cable and the aluminum tube, so that oscillation of this line
is limited (the outer shield of the cable being tested is short-circuited
to the tube at the instrumentation box). The current flowing on the
shield of the 3.2-meter-long test cable is measured with a Pearson Model
310 current probe near the instrumentation box. The shields and the co-
axial center conductors are short-circuited to one another at the end of
the cable where the spark-gap electrode is attached. The core wires and
shields are open-circuited inside the instrumentation box.
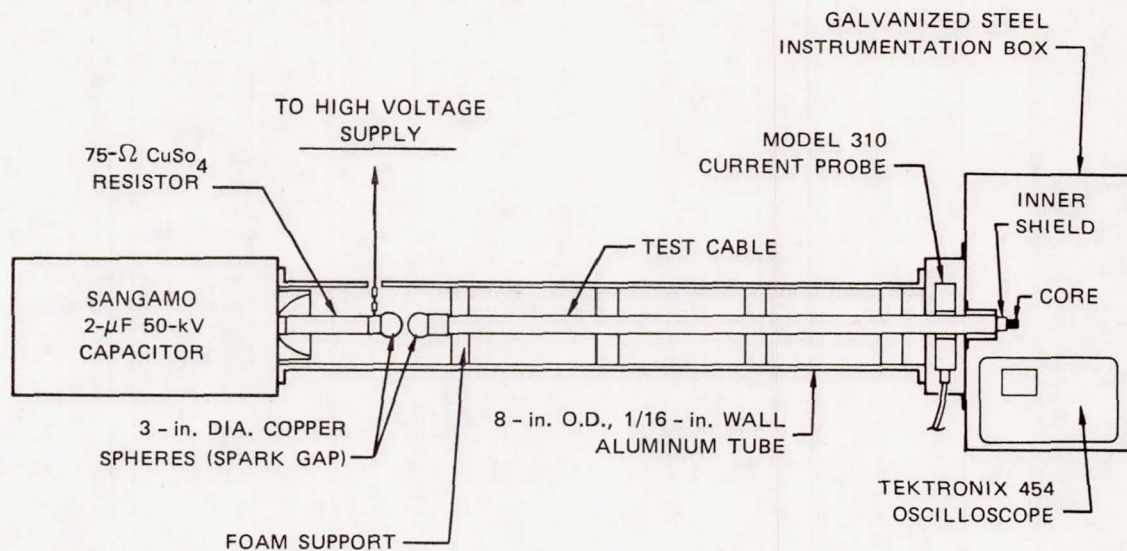
FIGURE A-1   LABORATORY TEST APPARATUS FOR MEASURING TRANSFER IMPEDANCE

A typical current pulse produced in the test-cable shield is shown in Figure A-2. The pulse rise time is about 20 ns (the rise time of the Pearson Model 310 current probe), and the decay time-constant is about 140 µs.

Cable Characteristics

The work discussed in this appendix was undertaken to determine the shielding effectiveness of two cables with different shield designs.

The construction of Cable 1 is shown in Figure A-3. This cable has a double shield: an outer shield of 24-mil-thick copper and an inner shield of 24-mil-thick mild steel. Both shields have continuously welded seams so that they behave electrically as solid-walled shields. This would correspond to the impractical case of an aircraft built without apertures such as windows or radomes.

The construction of Cable 2 is shown in Figure A-4. This cable also has a double shield: an outer shield composed of a double layer of counter-spiraled, copper-clad steel straps and an inner shield of 6.5-mil-thick mild steel with a longitudinal overlapped seam. This cable simulates

68

40 A

10 μs→

40 A

100 μs→
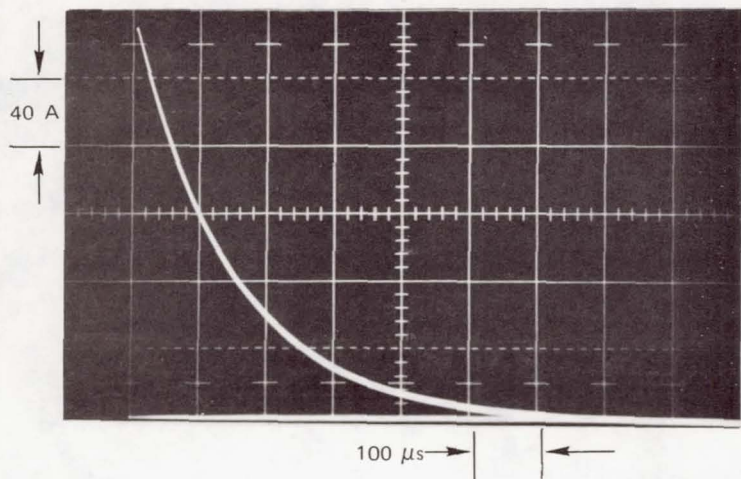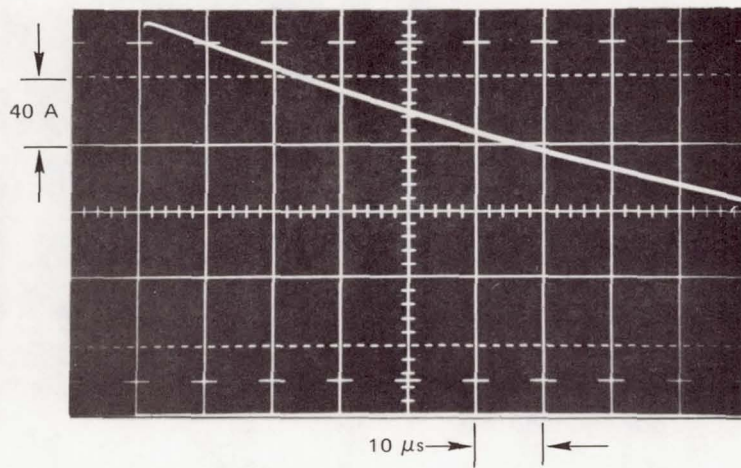
TA-1404-3

FIGURE A-2   CURRENT WAVEFORM IN CABLE SHIELD

69

OUTER SHIELD

Corrugated Copper,
2.65" O.D., 24 mil Thick

INNER SHIELD

Corrugated Steel,
2.17" O.D., 24 mil Thick

CORE

Coaxial Tubes,
Interstitial Pairs

OUTER JACKET

Semi-Conducting Polyethylene,
2.80" O.D., 70 mil Thick
Twelve 16 gauge wires
embedded in jacket

INNER JACKET

60 mil Polyethylene

INTERSTITIAL PAIRS

19-Gauge Conductors,
Polyethylene Jacket,
4 to 12 Pair in Cable

COAXIAL TUBE

Polyethylene Jacket, 0.750" O.D.
Outer Copper Conductor, 10 mil Thick
Inner Conductor, 0.160" O.D.
Polyethylene Dielectric, 0.620 O.D.

TA-1404-1

FIGURE A-3   CUTAWAY SHOWING CONSTRUCTION OF CABLE 1

OUTER SHIELD

Armor — two layers of 0.050" x 0.200" strips of 40% Copperweld, 25 in inner layer, 26 in outer layer, lay lengths about 15 inches, 1.94" O.D.

INNER SHIELD

Steel, 1.50" O.D., 6.5 mil Thick

INNER JACKET

90-mil Polyethylene

CORE

Coaxial Tubes, Twisted Pairs, Flood Filled

OUTER JACKET

Semi-Conducting Polyethylene, 2.14" O.D., 100 mil Thick

MIDDLE JACKET

120-mil Polyethylene

TWISTED PAIRS

19-Gauge Conductors, Polyethylene Jacket, 4 to 12 Pair in Cable

COAXIAL TUBE

Polyethylene Jacket, 0.465" O.D.
Outer Aluminum Conductor, 8 mil Thick
Inner Conductor, 0.0757" O.D.
Polyethylene Dielectric, 0.350 O.D.

TA-1404-2

FIGURE A-4   CUTAWAY SHOWING CONSTRUCTION OF CABLE 2

the electromagnetic character of a practical airplane that incorporates apertures in the skin.

The tests described here were designed to determine the leakage through the outer shields of these cables, and the oscilloscope was connected to measure the voltage between the inner and outer shields.

Test Results

The shield-to-shield voltage pulses measured under the conditions described above are shown in Figures A-5 and A-6 for Cables 1 and 2, respectively. The pulse response of Cable 1 shown in Figure A-5 illustrates the effect of the copper outer shield in filtering out the effects of the large dI/dt in the driving (shield) current, because the rise time of the voltage in Figure A-5 is about 10 μs, compared with 20 ns for the current.
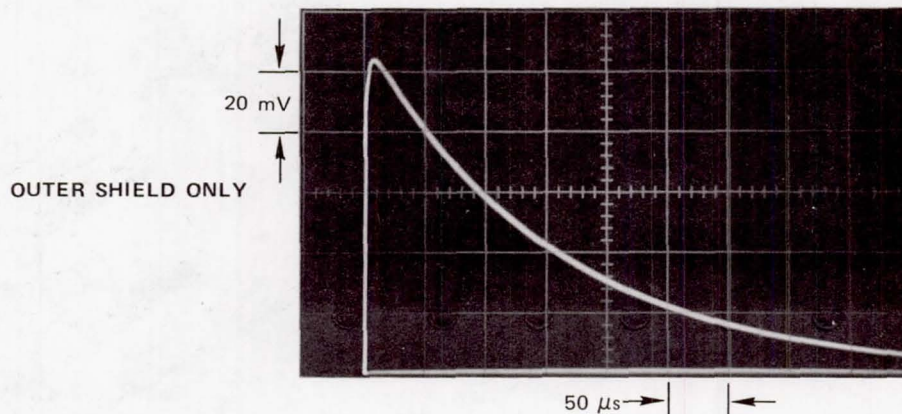
FIGURE A-5   INTERNAL VOLTAGES PRODUCED IN CABLE 1
BY A 220A PEAK-CURRENT PULSE

The response of Cable 2 is quite different from that of Cable 1, as is apparent from comparing Figures A-5 and A-6. This difference is caused primarily by the construction of the outer shield of Cable 2, which permits some of the large dI/dt energy to penetrate to the interior of the cable. The penetration of the fast-rising portion of the pulse is apparent in Figure A-6, where it is seen that the voltage developed between the two shields has a fast-rising negative pulse, followed by the slower, diffusion-controlled positive pulse.

72

50 mV

OUTER SHIELD ONLY

50 μs →| |←
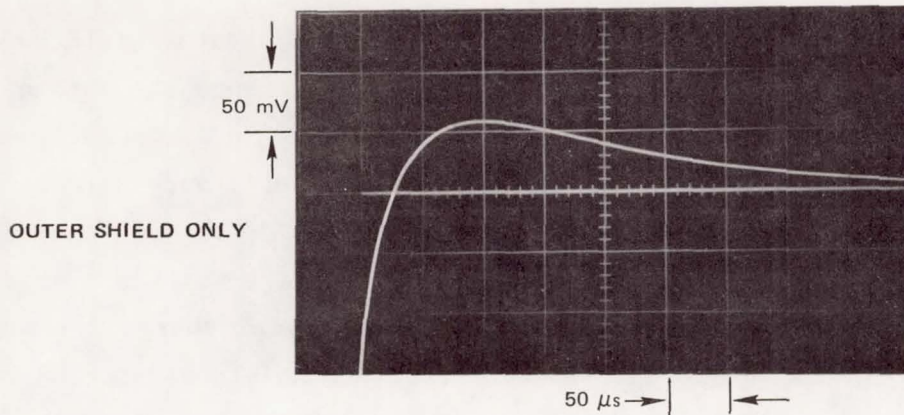
FIGURE A-6   INTERNAL VOLTAGE PULSES PRODUCED IN CABLE 2
BY A 184A PEAK-CURRENT PULSE

That the outer shield of Cable 2 permits penetration of the high
frequencies (large dI/dt) is apparent in Figure A-7, where the leading
edge of the pulse of Figure A-6 is shown greatly expanded. Here it can
be seen that a damped 24-MHz oscillation dominates the leading edge of
the pulse (24-MHz is the quarter-wave resonance frequency of the shorted
3.2-meter-long cable). In Figure A-7, the peak voltage of the 24-MHz
oscillation is over 3 volts, whereas the peak of the diffused pulse after
the oscillations have subsided is less than 0.1 volt in Figure A-6. The
voltage at the resonance frequency is thus enhanced by a factor of about
30 over the remainder of the response.

1 V

OUTER SHIELD ONLY

100 ns →| |←
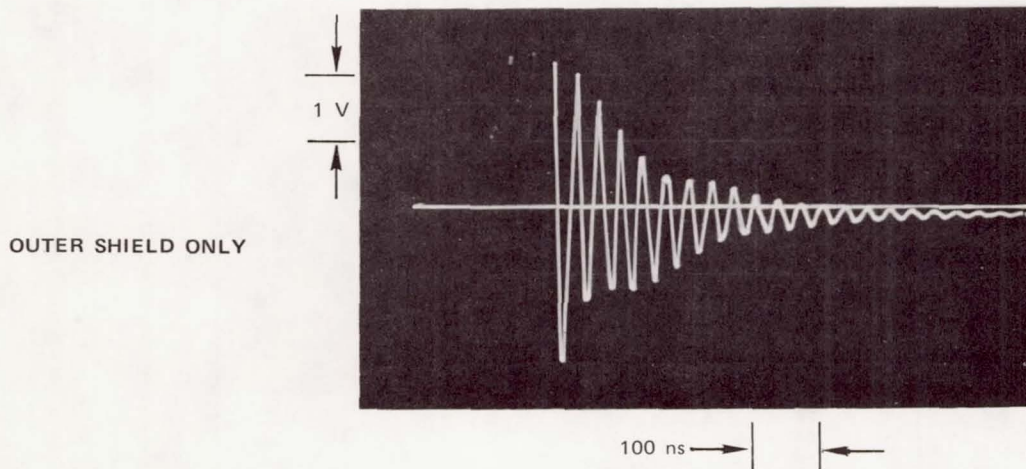
FIGURE A-7   LEADING EDGES OF THE INDUCED-VOLTAGE PULSE OF FIGURE A-6

73

These results clearly illustrate the effect of the shield imperfections on the electromagnetic energy that leaks through the shield. This leakage, which occurs through apertures or cracks in the shield, can be represented by a mutual inductance and mutual capacitance between the circuit inside the cylinder and the circuit outside the cylinder. Thus, the voltage induced by the shield current I_s can be written $V = j\omega M I_s$, and the current induced by the shield voltage V_o (or charge Q_o) can be written $I - j\omega C\ V_o = j\omega C\ Q_o/C_o$. Hence, if the shield excitation contains high frequencies, these high frequencies tend to dominate the internal conductor response. This dominance was noted in the test results for Cable 2 even though its shield had almost 100% optical coverage. Similar responses are to be expected for aircraft fuselage and wing wiring because of windows, access plates, and riveted or bolted joints in the skin.

Results similar to these have been reported recently by Plummer,[17] Butters and Clifford,[18] and Burrows et al.[19]

Appendix B

LABORATORY AND FLIGHT TEST CALIBRATIONS OF INSTRUMENTATION
SENSORS AND ELECTRONIC SYSTEMS

Appendix B

LABORATORY AND FLIGHT TEST CALIBRATIONS OF INSTRUMENTATION
SENSORS AND ELECTRONIC SYSTEMS

General

Calibrations and functional tests of the sensors and instrumentation
were carried out throughout the program. In general, the passive sensors
were calibrated prior to the flight period either by analysis or by using
laboratory setups to generate known transient fields. Because the response
of these sensors is determined by their physical configuration, it remains
constant unless the form of the sensor is changed. Accordingly, during
the flight test program, only functional tests of these sensors were
carried out.

All of the electronic systems and the active sensors such as the
field mills were calibrated on a regular basis throughout the entire flight
test program.

The calibration procedures followed during system fabrication and
during the flight test period will be discussed in this appendix.

Static Electric Field Meter System Checks and Calibrations

Laboratory Calibrations

The purpose of the field-meter system is to measure the static
electric field structure in the vicinity of the thunderstorm cell under
investigation. Because the airplane used to carry the sensors distorts
the free space fields, it in effect becomes part of the sensor system,
and must be included in the calibration. The laboratory procedure fol-
lowed in determining field distortions caused by airplane geometry was
described in considerable detail in Reference 1. An abbreviated descrip-
tion will be given here together with the new matrix of constants used
in designing the analog data processor for the 1977 flight tests. (The

77

mounting location of one of the field meters was moved for this test program, necessitating a different set of parameters than was used in 1975 and 1976.)

The static field perturbation produced by an aircraft is illustrated in Figure B-1 for the case of an aircraft introduced into a uniform field with the aircraft roll axis along the direction of the field lines. The measurement system must be capable of reconstructing the free-space field components from the fields measured at the surface of the aircraft. From Figure B-1, it is evident that the normal surface field E_N is greater than the ambient field E_o at the nose of the aircraft and at the tail. Also, the sign of the surface field at the nose is opposite to that at the tail. Near the middle of the fuselage, $E_N = 0$. Thus, the field structure at the surface of the aircraft is affected by the geometry of the aircraft. Specifically, the magnitude and sign of E_N/E_o at each point is uniquely determined by the aircraft geometry. In particular, the relationships E_N/E_o can be determined (by using scale-model measurements) and then applied to the full-scale aircraft.

Siting field-meter sensors on the aircraft involves practical considerations such as structure, access, and cabling. Within these restrictions, positions are chosen where the local field depends most strongly on one of the principal field components. The locations chosen for the
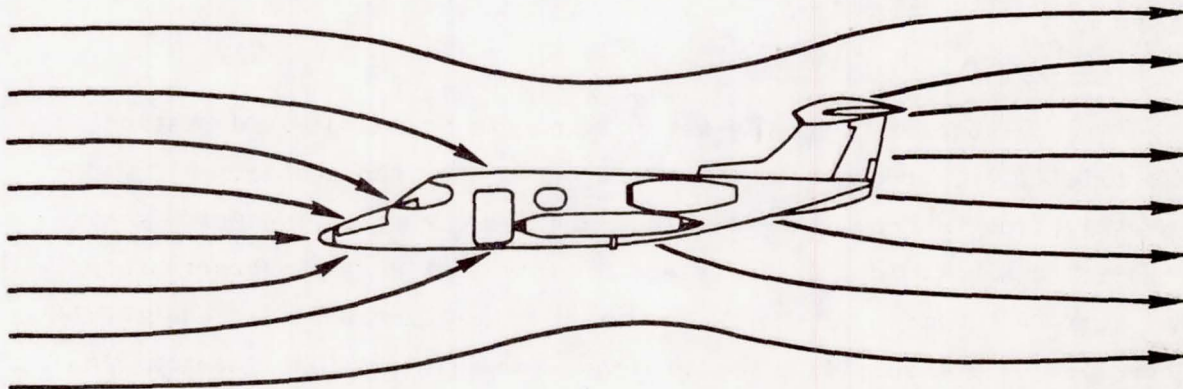
SA-5537-26

FIGURE B-1   PERTURBATIONS OF UNIFORM ELECTRIC FIELD CAUSED BY AN AIRCRAFT

1977 tests are shown in Figure 2 (Section II of the main body of the report). The field meter on the fin cap was used only as a backup sensor.

Given the field-meter sensor locations, it is necessary to express the field-meter readings in terms of free-space fields. For certain simple geometries, this can be done analytically. For the complex geometry of the Learjet, a modeling approach to the determination was used, as is illustrated in Figure B-2. An electrically conducting model of the aircraft was suspended in the uniform field between a pair of charged, electrically conducting plates. The field pattern about the model duplicates the structure that would exist about the full-scale aircraft (see Figure B-2).

The relationship between the local field normal to the skin, E_N, and the free space field, E_o, is determined by charge transfer measurements. If a small metal probe supported on a good insulator is touched to the model at a point of interest, it will acquire a charge q_N given by

$$q_N = \epsilon_o A E_N \qquad (B-1)$$

where $\epsilon_o = 1/36\pi \times 10^9$ farad/m is the dielectric constant of free space, and A is the induction area of the test probe. If the same probe is now touched to one of the end plates, where the field intensity is E_o, it will acquire a charge q_o given by

$$q_N = \epsilon_o A E_o \qquad . \qquad (B-2)$$

Thus, the relationship of local surface field to ambient field is simply the ratio of charges transferred in the model measurements

$$\frac{E_N}{E_o} = \frac{q_N}{q_o} \qquad . \qquad (B-3)$$

Charge transfer measurements were made at each of the four field-meter locations. Following each set of measurements, the model was re-oriented so that ultimately a set of measurements was generated with each

PLATE
ELECTRODE

INSULATING ROD

SMALL METAL PROBE

PLATE
ELECTRODE

AIRCRAFT MODEL ON
INSULATING SUPPORT

HIGH-VOLTAGE
POWER SUPPLY

FARADAY ICE PAIL

GENERATING
VOLTMETER
ELECTROMETER
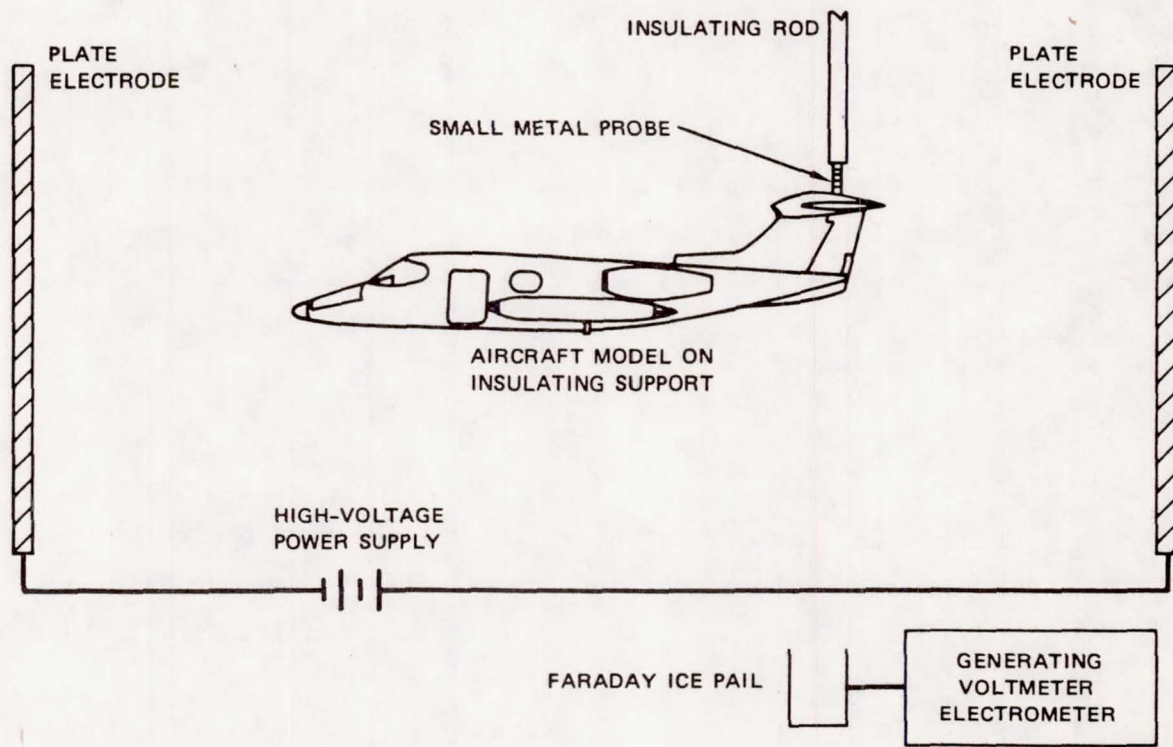
SA-5537-28

FIGURE B-2   AIRCRAFT CALIBRATION IN ELECTROSTATIC CAGE

of the three principal aircraft axes along the direction of the field in the electrostatic cage.

The sets of equations generated by using this procedure are shown in Table B-1. Essentially, measurements conducted with $E_x \neq 0$ yield values for a_1, a_2, a_3, and a_4. Similarly, measurements with $E_y \neq 0$ yield b_n, and measurements with $E_z \neq 0$ yield c_n. The values for d_n are determined by suspending the model in free space and repeating the charge transfer measurements with the aircraft model suspended in free space and charged to a known potential V.

Table B-1

FIELD CALIBRATIONS MATRIX FOR TEST AIRCRAFT

$$E_{RIGHT} = a_1 E_x + b_1 E_y + c_1 E_z + d_1 V$$

$$E_{FORE} = a_2 E_x + b_2 E_y + c_2 E_z + d_2 V$$

$$E_{AFT} = a_3 E_x + b_3 E_y + c_3 E_z + d_3 V$$

$$E_{LEFT} = a_4 E_x + b_4 E_y + c_4 E_z + d_4 V$$

The model measurement data presented in the form of the matrix of Table B-1 express the field-meter readings in terms of the free-space field components. For the flight test applications, this matrix was inverted to express the free-space fields in terms of the four field-meter readings, as is shown in Table B-2. Although the relationships of Table B-2 could be used on the ground at the completion of flight testing to convert field-meter readings to free-space fields, provisions were included in the field-meter system to do the processing in real time in flight. Thus, the Learjet instrumentation system included an analog data processor that used the constants of Table B-2 to combine the field-meter outputs in such a way that the three free-field components and airplane potential were displayed and recorded directly in flight.

Dynamic range is achieved by using a set of four synchronous detectors for each sensor to produce a set of four linear output ranges. The

Table B-2

INVERTED MATRIX OF LEARJET FIELD-METER CALIBRATION
FOR 1977 FLIGHT TESTS

$$E_X = 0.0526 \; E_R + 0 \; E_{FOR} + 0 \; E_{AFT} - 0.0526 \; E_{LEFT}$$

$$E_y = 0.0045 \; E_R + 0.5059 \; E_F - 0.4861 \; E_A + 0.0045 \; E_L$$

$$E_z = 0.0655 \; E_R - 0.5724 \; E_F - 0.0338 \; E_A + 0.0655 \; E_L$$

$$V = -0.4206 \; E_R + 1.9342 \; E_F - 1.9964 \; E_A - 0.4206 \; E_L$$

proper operating range for the ambient field levels is selected by
the flight test observer.

Flight Test Calibration

The field-meter system was calibrated before and after each flight.
In this way, there was never any question regarding the proper function-
ing of the instrumentation for more than a portion of a single flight.

Calibration was accomplished by establishing a known electric field
intensity over a field-meter sensor and recording the resulting output
on a strip-chart recorder. In this way, all elements of the system from
the sensor head through the field-meter electronics and data processor
to the recorder were included in each calibration. Any deviation from
normal behavior of any of these elements is immediately apparent. In
general, the field-meter system was found to be very stable and reliable.

Calibration factors were obtained as follows: Assuming that a field
$E_N = 1$ kV/m is established over the forward belly field meter (with the
remaining fields equal to zero) and the E_y channel output is monitored,
from the second equation of Table B-2 we find that

$$E_y = 0.506 \; E_{FOR} \qquad . \tag{B-4}$$

Thus, the calibrating signal and the resulting recorder deflection cor-
responds to a free-space field $E_y = 0.506$ kV/m.

The calibrating field was generated at a field-meter position by locating a metal sheet 10 cm above the aircraft skin (using 10-cm-long standoff insulators) and applying a voltage V between the calibrating plate and the skin. The calibrating field is given by

$$E_{CAL} = V/0.1m \quad . \qquad (B-5)$$

The calibration source used for this purpose includes provisions for stepping the calibration field through several ranges of values to check system linearity. It also includes high-value series resistors to reduce the output voltage to zero if any applicable current is drawn from the calibrator.

Transient Sensors

Laboratory Checks and Calibrations

E-Field Antenna System

As indicated in Section II under "Sensors," the E-field antenna has the simple equivalent circuit given in Figure 3. The values of the parameters for the specific antenna used in the test program were determined from the experimental data published by Bolljohn.[7]

Skin Current Sensors

- Half loops. As is indicated in Section II, the properties of the simple half-loop antenna are sufficiently well understood that calibration factors based on the calculated characteristics of these antennas can be used with confidence. Accordingly, no experimental measurements were made to confirm the half-loop calibration.

- Slot antennas. To determine the calibration of the slot antennas, one of the flight units was installed in the wall of the rectangular coaxial skin tester described in Reference 20. The design of the tester is such that a TEM wave is propagated between each of the flat outside walls and the flatsheet center conductor thereby generating a region of uniform field. The system is designed to be a 50-ohm structure over the range 10 kHz to 100 MHz.

  For the slot antenna calibrations, the rectangular coaxial tester was driven with a fast-rising step pulse. The waveform of the

83

driving pulse was recorded on a two-channel oscilloscope, together with the slot antenna output pulse. From the amplitude and rise-time of the driving pulse and the design of the coaxial tester, it was possible to determine dJ/dt. This, combined with the antenna output pulse amplitude, yielded the slot antenna calibration.

H-Field Antenna System

The multi-turn loop used in the nose of the aircraft to measure the magnetic field of incident lightning pulses consisted of three turns of AWG 12 wire with a mean loop diameter of 18 inches. The short-circuit current of the loop was measured with a Tektronix CT-2 current probe. The magnetic field intensity is

$$H = \frac{L}{\mu A} I \quad . \tag{B-6}$$

For the nose loop, $L \approx 6.5$ μH and $L/\mu A \approx 26.5$ m^{-1}. The CT-2 delivers 1 V/A, so that the short-circuit current, I, may be replaced by the CT-2 voltage, V_{CT}. Thus the calibration for this loop is given by

$$H = 26.5 \ V_{CT} \quad . \tag{B-7}$$

The low-frequency limit on the nose loop's performance was determined to be about 4 kHz from laboratory measurements. The effect of the bulkhead on the sensitivity and low frequency limit were not determined.

Wire Pickup Sensors

Because these sensors were intended to be representative of typical wiring inside an aircraft, no special designs or calibrations of the installation were undertaken.

Flight Test Checks and Calibrations

E-Field Antenna--Direct Drive

The functioning of the E-field antenna was checked and the preamplifier calibration was verified for each flight during the flight test

program by applying a train of pulses to the antenna terminal through a 5-pF capacitor (as shown in Figure B-3) and observing the output from the preamplifier on an oscilloscope. From the equivalent circuits shown in Figure B-3, it is possible to establish an equivalence between the calibration voltage and electric field required to produce the same input to the preamplifier as follows:

$$V_{cal} \frac{5}{5 + C_L} = Eh_e \frac{7.8}{7.8 + C_L} \quad . \tag{B-8}$$

Because the system was designed so that $C_L \gg 7.8$, this can be rewritten

$$E = \frac{5}{7.8} \frac{V_{cal}}{h_e} \quad . \tag{B-9}$$

Because $h_e = 0.17$ meters, this becomes

$$E = \frac{5}{7.8} \frac{V_{cal}}{0.17} \tag{B-10}$$

or

$$E = 3.77 \ V_{cal} \quad . \tag{B-11}$$

The major advantage of the direct-drive calibration scheme is that it accounts for preamplifier gain, attenuators, and power splitters in the circuit.

E-Field Antenna--Spectrum Analyzer Injection

Occasionally, it is desirable to determine E-field antenna system calibration by injecting the test signal into the spectrum analyzer input. This can be accommodated by using the results of the direct-drive tests of Figure B-3. During a typical direct-drive calibration, a 20-volt pulse was used ($V_{cal} = 20V$) that, substituting into Equation (B-11), yields an equivalent calibration field $E_{cal} = 20(3.77)$. With this calibration signal applied, the preamplifier output pulse amplitude was measured. The results are listed in the third column of Table B-3. Dividing the calibration field by the observed output yields the final calibration shown
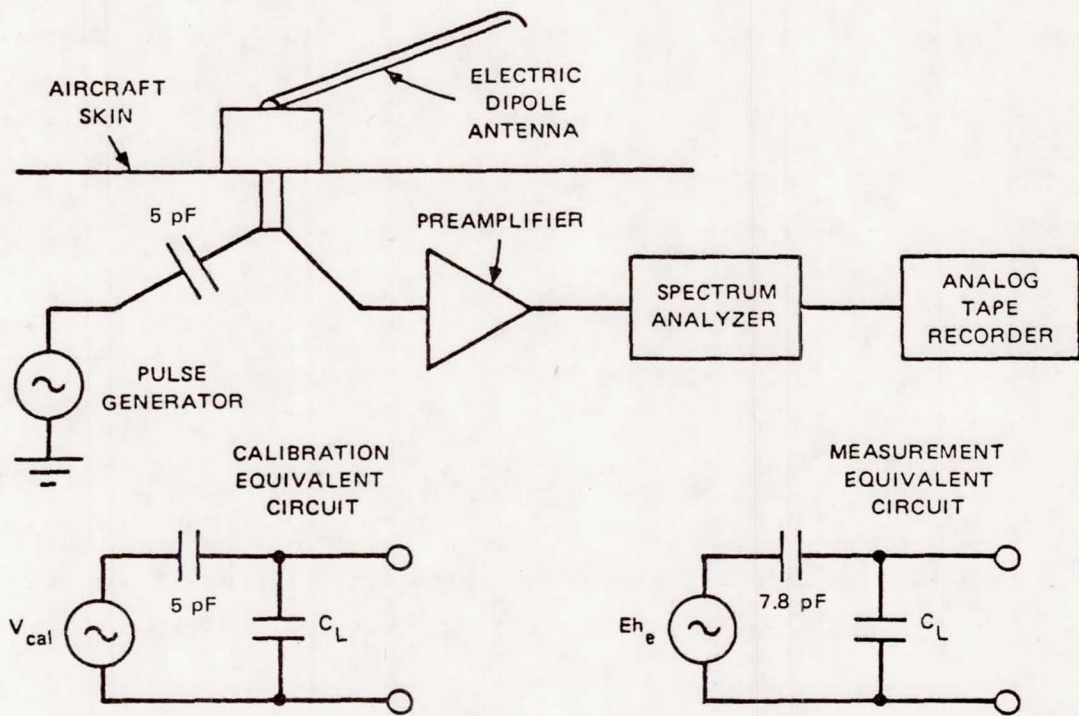
85

FIGURE B-3   PREFLIGHT CALIBRATION OF ELECTRIC-DIPOLE SPECTRUM ANALYZER SYSTEM

Table B-3

CALIBRATION OF E-FIELD DIPOLE ANTENNA AND PREAMPLIFIER SYSTEM
FOR SPECTRUM ANALYZER SIGNAL INJECTION

Switch Position	Nominal Attenuation (db)	Preamp Output (mV)	Calibration E(V/m)
1	0	200	$377 \ V_{out}$
2	20	18	$4200 \ V_{out}$
3	40	1.8	$4.12 \times 10^4 \ V_{out}$

in the last column of the table. For example, for switch setting No. 1, V_{out} = 0.2 volt so

$$\frac{E}{V} = \frac{20(3.77)}{0.2}$$

$$= 377 \ V_{out} \quad .$$

(B-12)

H-Field Antenna

The H-field antenna located at the nose of the aircraft was given a functional test prior to each flight by using a pulsed loop that was placed over the outside of the radome. Again, during these system checks, no effort was made to relate the test signal directly to a propagating H-field.

Wire Pickup Sensors

Periodic functional checks were made of the wires to verify that terminations were still intact.

Spectrum Analyzer System

The calibration technique used for the spectrum analyzer system is best understood when viewed in light of a functional description of a

87

typical spectrum analyzer channel. A functional circuit of a channel
is shown in Figure B-4, together with an indication of the waveforms
expected at various points in the system in response to an input transient
signal. The input transient pulse is amplified and applied to a tuned
circuit. The tuned circuit extracts energy from the driving pulse and
generates a damped oscillation. The frequency of the oscillation is
determined by the resonant frequency of the circuit. The decay time of
the damped oscillation is determined by the Q of the tuned circuit, and
the amplitude of the oscillation is proportional to that energy in the
original pulse contained within the passband of the tuned circuit. The
damped oscillatory signal is rectified and smoothed to generate the in-
dicated output pulse, whose length is determined by tuned circuit and
output filter characteristics and whose amplitude is proportional to
the amplitude of the input signal.

The flight test calibration of the spectrum analyzer was accomplished
by applying a train of pulses to the spectrum analyzer input and recording
the resulting output pulses on the analog tape recorder. The pulse rise-
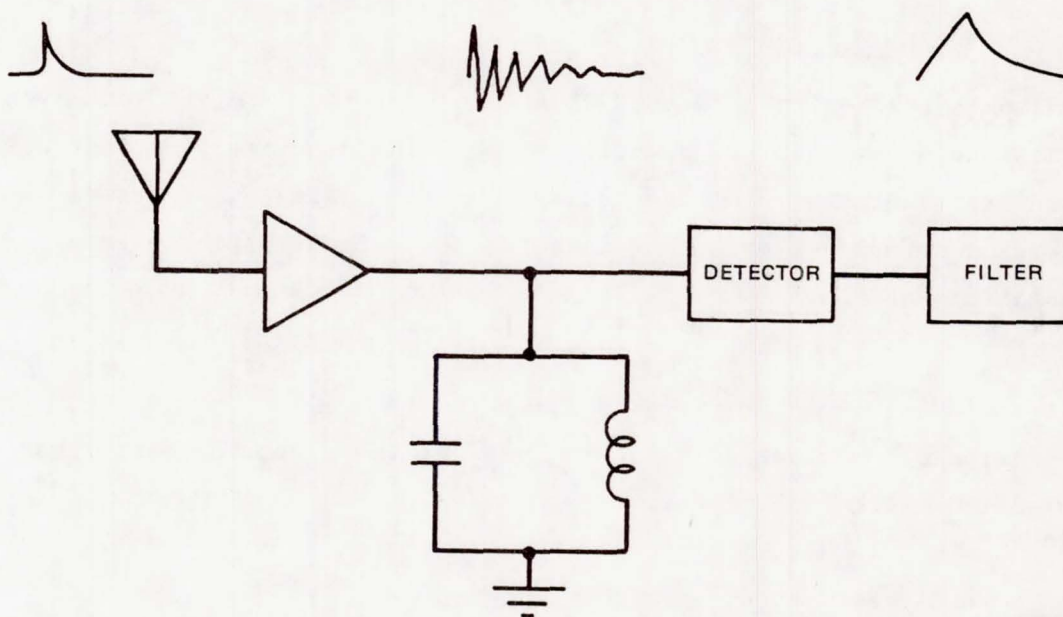time and durations were chosen to allow a simple interpretation of the

FIGURE B-4   FUNCTIONAL DIAGRAM OF SPECTRUM ANALYZER

excitation function so that the spectrum analyzer response to the calibrating signal could be applied to other signals. The form of the calibrating signal used is shown in the upper part of Figure B-5; this form was chosen for the following reason.
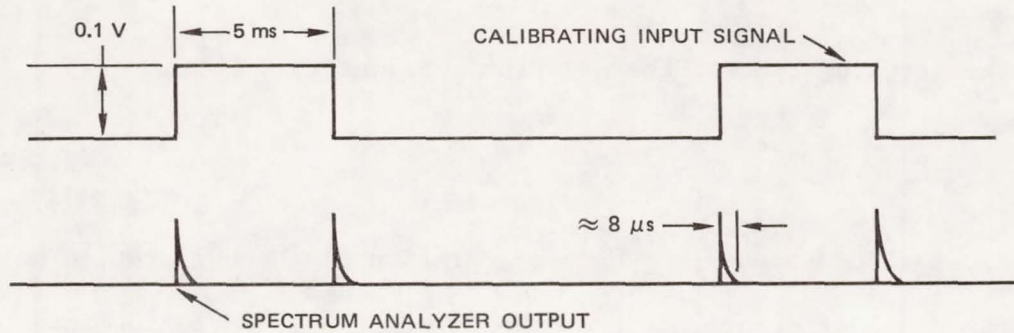
FIGURE B-5 SPECTRUM ANALYZER CALIBRATION SIGNAL AND RESPONSE

The step is a clearly-defined function with the very simple Fourier transform $G(\omega)$ given by

$$G(\omega) = \frac{A}{\omega} \tag{B-13}$$

where A is the amplitude of the step. Unfortunately, a true step function is awkward to use because it occurs only once. In practice, the step can be approximated by a rectangular pulse, provided that the duration of the pulse is long compared with the response time of the spectrum analyzer. If this condition is fulfilled, the following sequence of events will occur. The spectrum analyzer tuned circuit will be excited into damped oscillation by the leading edge of the pulse. This oscillation will be rectified and filtered, producing the first output pulse shown in the bottom line of Figure B-5. By the time the trailing edge of the rectangular driving pulse arrives, the spectrum analyzer system will be in a quiescent state. As is indicated in Figure B-5, the trailing edge of the input pulse produces a second output pulse identical to the first.

89

The flight test spectrum analyzer system was designed to have a frequency response consistent with the available 20 kHz bandwidth of the analog tape recorder. The settling time constant τ associated with a particular upper frequency f is given

$$\tau \approx \frac{1}{2\pi f} \quad . \tag{B-14}$$

Thus, the settling time of the spectrum analyzer will be

$$\tau \approx \frac{0.159}{2 \times 10^4} = 8 \ \mu s \quad , \tag{B-15}$$

which is small compared with the 5 ms duration of the calibration pulse.

This calibration procedure can be directly applied to the interpretation of the flight-test data as follows. Assuming that, in flight, the spectrum analyzer channel of Figure B-5 is connected to the E-field antenna system with the gain switch on position 1. The calibrating signal is equivalent to an identical output pulse from the E-antenna preamplifier. From the last column in Table B-3, we find that for switch position 1, the corresponding electric field at the antenna is given by

$$E = 377 \ V \quad . \tag{B-16}$$

Because our calibrating signal step amplitude is 0.1 volt, this corresponds to an electric field step at the antenna of

$$E = 0.1(377) = 37.7 \ V/m \quad . \tag{B-17}$$

If the spectrum analyzer channel is tuned to a center frequency of 10 MHz, the corresponding field spectral density $G(\omega)$ can be found by using Equation (B-13) to take the Fourier transform of this field step.

$$G(\omega) = \frac{A}{\omega} = \frac{37.7}{6.28 \times 10^7}$$
$$= 6 \times 10^{-7} \ \frac{V - s}{m} \quad . \tag{B-18}$$

90

Thus, the output pulse on the lower line in Figure B-5 can be interpreted as the response of the system to a transient event that generates a field spectral density of $6 \times 10^{-7} (V - s)/m$ at 10 MHz.

Magnetic-field spectral-density calibrations for the nose loop can be obtained in a similar manner using the calibrations of Equation (B-7) in place of the data from Table B-3.

If the spectrum analyzer channel were tuned to 10 MHz and were used with one of the skin current sensors such as the slot antenna, the following procedure would be followed: From Equation (6) in Section II of the report, we find that

$$\dot{J} = \frac{V}{\ell_e L} \quad , \tag{6}$$

and from Equation (8), we obtain for the slots used in the Learjet tests the following calibration constant

$$\frac{1}{\ell_e L} = 912 \times 10^6 (H - m)^{-1} \quad . \tag{8}$$

Combining Equation (6) and Equation (8) yields

$$\dot{J} = 912 \times 10^6 V \quad , \tag{B-19}$$

which, for a calibrating step voltage $V = 0.1$, becomes

$$\dot{J} = 912 \times 10^5 \quad . \tag{B-20}$$

With the use of Equation (B-13), the Fourier transform of a step of this magnitude is given by

$$\dot{J}(\omega) = \frac{912 \times 10^5}{\omega} \quad . \tag{B-21}$$

91

From Fourier transform theory, the transform of a function can be obtained from the transform of its deviation by dividing ω as follows:

$$J(\omega) = \frac{1}{\omega} \dot{J}(\omega) \quad . \tag{B-22}$$

Applying the relationship of Equation (B-22) to Equation (B-21) yields

$$J(\omega) = \frac{912 \times 10^5}{\omega^2} \quad , \tag{B-23}$$

which for a spectrum analyzer frequency of 10 MHz becomes

$$J(\omega) = \frac{912 \times 10^5}{(6.28 \times 10^7)^2}$$

$$= 2.3 \times 10^{-8} \frac{A - s}{m} \quad . \tag{B-24}$$

Thus, the output pulse on the lower line of Figure B-5 can be interpreted as the response of the system to a transient event that generates a field spectral density of 2.3×10^{-8} (A - s)/m at 10 MHz.

The calibration data can be interpreted in still another way, as illustrated in the case of the cabin wire current record near the bottom of Figure 12 of Section IV. In this case, the calibration units are given simply as amperes, and represent the current step in the wire required to produce the same response in the spectrum analyzer channel. (This was done to provide perspective and physical insight into the levels of signals involved.) If the 0.1-volt calibrating signal was generated at the output of a CT-2 current transformer installed on a wire, the calibrating signal step and corresponding output pulse would be equivalent to a 0.1 ampere current step in the wire.

Charging Patch System

The charging patch system shown in Figure 7 of Section II was calibrated by attaching a battery through a series resistor to the sensor on the tank tip to drive a known current into the sensor. The system output was recorded on the analog tape during calibration.

Appendix C

FIELDS CAUSED BY LIGHTNING

Page intentionally left blank

Appendix C

FIELDS CAUSED BY LIGHTNING

If M_t is the electric moment of a thundercloud at time t, then the vertical electric field E_t at a distance d from a storm is given approximately by

$$E_t = \frac{1}{4\pi\varepsilon_o}\left(\frac{M_t}{d^3} + \frac{1}{cd^2} \cdot \frac{dM_t}{dt} + \frac{1}{c^2 d} \cdot \frac{d^2 M_t}{dt^2}\right) \quad . \qquad \text{(C-1)}$$

Equation (C-1) was originally discussed in relation to thunderstorm electricity by Lejay.[21] It applies reasonably well over distances long enough to make ionospheric influences of little importance; the appropriate distance range might be defined as 20 to 200 km. In Equation (C-1), c is the velocity of light (3×10^8 m/s), t represents time, and ε_o is the permittivity of free space $(36\pi \times 10^9)^{-1}$. If MKS units are used throughout Equation (C-1), the field E is in volts per meter (V/m). The three terms of Equation (C-1) are often known as the "electrostatic" (M_t), "induction" (dM_t/dt), and "radiation" ($d^2 M_t/dt^2$); the latter are usually only of significance when a lightning flash is occurring and M_t is therefore changing rapidly. Equation (C-1) considers the propagation to be over a perfectly conducting earth. Strictly speaking, the values of M_t etc. should be those at the retarded time (t - d/c) and not at time t.

The moment M_t is defined as the summation at time t of Σ 2qh, where q is the charge and h is the height of an elementary charge. The summation extends over all charges associated with a thundercloud. Two types of lightning flash are especially common: the discharge to earth, and the discharge within the cloud. Before a flash occurs, the charge distribution in the cloud is approximately represented very simply in a surprisingly large number of instances by point charges +Q and -Q located at heights of 2H and H respectively;[22] the corresponding cloud moment is therefore 2QH. When an intracloud discharge occurs, the result is

effectively a mutual neutralization of the cloud charges. For the discharge to earth, the lower charge −Q passes to ground. In each case, the change in moment is the same in magnitude (2QH). It is, however, opposite in sign with the intracloud discharge, from Equation (C-1), giving a negative* electrostatic field change of $1/(4\pi\varepsilon_o)$ $(2QH/d^3)$; the flash to earth produces a positive field change of equal size.

It has been suggested that Equation (C-1) applies only for d = 20 to 200 km. The deviations with small d from the electrostatic field change given by Equation (C-1) are not too serious for flashes to earth, but are very considerable in the case of the intracloud discharge; there is even a reversal in field. With the thundercloud charge model specified above, the electrostatic field changes for intracloud ($_cE_s$) and ground discharge ($_GE_s$) are given by

$$_cE_s = \frac{1}{4\pi\varepsilon_o}\left[\frac{2QH}{(d^2 + H^2)^{3/2}} - \frac{4QH}{(d^2 + 4H^2)^{3/2}}\right] \approx -\frac{2QH}{4\pi\varepsilon_o d^3} \quad \text{for large} \quad \text{(C-2)}$$

and

$$_GE_s = \frac{1}{4\pi\varepsilon_o}\left[\frac{2QH}{(d^2 + H^2)^{3/2}}\right] \approx \frac{2QH}{4\pi\varepsilon_o d^3} \quad \text{for large d} \quad . \quad \text{(C-3)}$$

In Figure C-1, $_GE_s$ and $_cE_s$ are plotted for Q = 20 coulomb and H = 3 km; these are not inappropriate values for a storm in temperate latitudes.[22] Evidently, the $1/d^3$ law is closely approached for both intracloud strokes and strokes to earth when d $\geq$ 20 km.

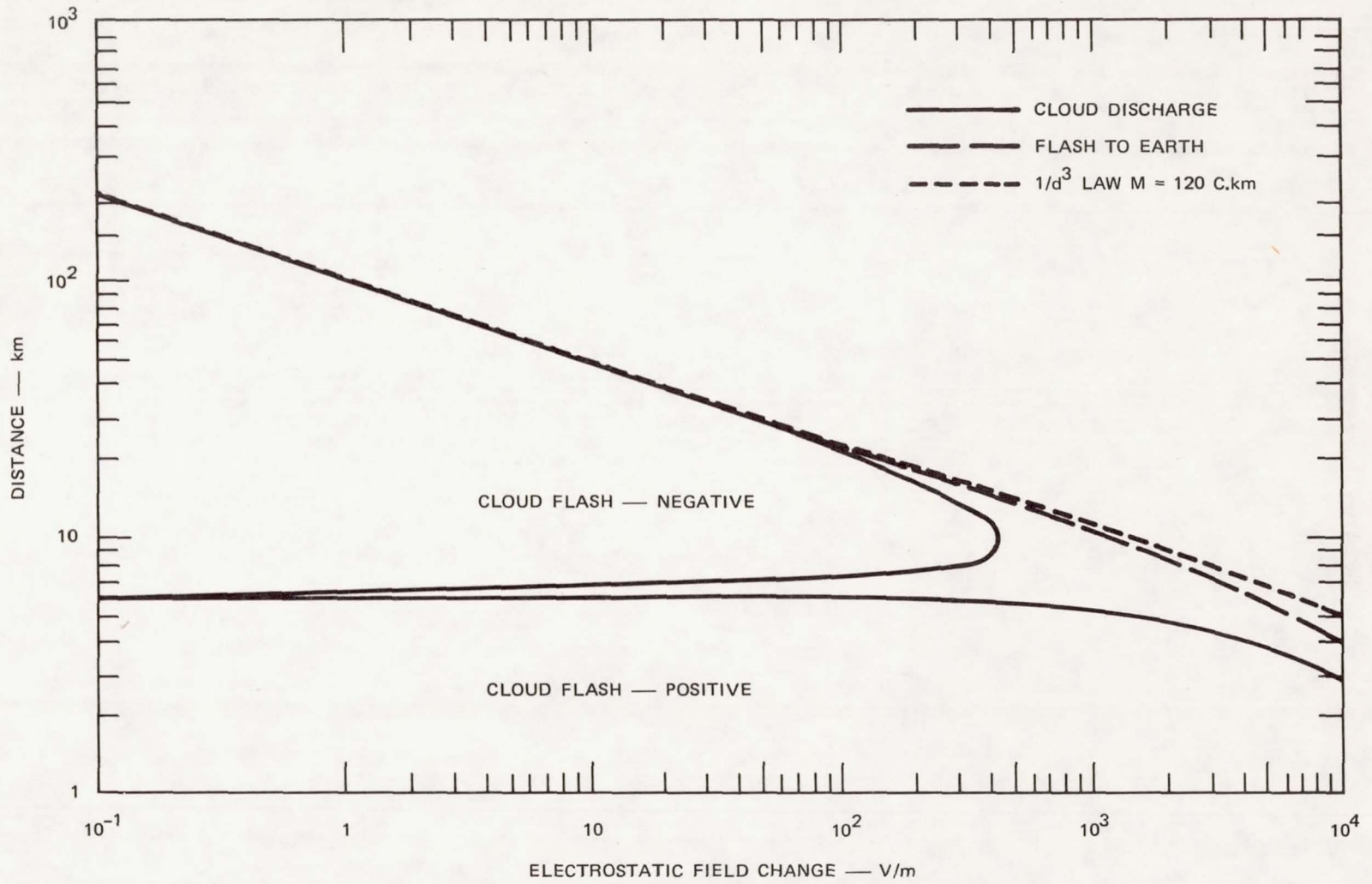
*Usual sign convention of atmospheric electricity.

FIGURE C-1 RELATIONSHIP BETWEEN ELECTROSTATIC FIELD CHANGE AND DISTANCE

REFERENCES

1. R. T. Bly, Jr., and J. E. Nanevicz, "Aerial Measurements of the Electric Field in the Vicinity of Florida Thunderstorms: Analysis and Results," Final Report, Contract NAS10-9013, SRI Project 5537, SRI International, Menlo Park, California (June 1977).

2. Donald D. Arabian, "JSC Thunderstorm Experiment Results," Report JSC-12509, National Aeronautics and Space Administration, Houston, Texas (March 1977).

3. J. E. Nanevicz, R. C. Adamo, and R. T. Bly, Jr., "Airborne Measurement of Electromagnetic Environment Near Thunderstorm Cells (TRIP-76)," Final Report, Contract NAS9-15101, SRI Project 5536, SRI International, Menlo Park, California (March 1977).

4. Jerome T. Dijak, "Airborne Measurements of Transient Electric Fields and Induced Transients in Aircraft Due to Close Lightning," Project 43630135, Air Force Flight Dynamics Laboratory, Wright-Patterson AFB, Ohio (June 1977).

5. N. Cianos and E. T. Pierce, "A Ground-Lightning Environment for Engineering Usage," Technical Report 1, Contract L.S.-2817-A3, SRI Project 1834, SRI International, Menlo Park, California (August 1972).

6. E. F. Vance, J. E. Nanevicz, and G. August, "Technical Inputs and EMP Design Practices for Intrasite Cabling of Telecommunication Facilities," Final Report, Contract DAAG39-76-C-0021, SRI Project 4587, SRI International, Menlo Park, California (June 1977).

7. J. T. Bolljahn, "Antennas for Airborne ADF Systems," Final Report--Task II, Contract AF-33(616)-83, SRI Project 606, SRI International, Menlo Park, California (July 1954).

8. R. L. Tanner and J. E. Nanevicz, "An Analysis of Corona-Generated Interference," _Proc. IEEE_, Vol. 52, No. 1 (January 1964).

9. J. E. Nanevicz and R. L. Tanner, "Some techniques for the Elimination of Corona Discharge Noise in Aircraft Antennas," _Proc. IEEE_, Vol. 52, No. 1 (January 1964).

10. R. L. Tanner and J. E. Nanevicz, "Precipitation Charging and Corona-Generated Interference in Aircraft," Technical Report 73, Contract AF 19(604-3458), SRI Project 2494, Stanford Research Institute, Menlo Park, California (April 1961).

11. J. E. Nanevicz, "Flight Evaluation of Induced-Noise Mechanisms on High-Speed Aircraft," AFAL-TR-73-317, SRI Project 7104, Stanford Research Institute, Menlo Park, California (October 1973).

12. N. Cianos, G. N. Oetzel, and E. T. Pierce, "Structure of Lightning Noise--Especially Above HF," AFAL-TR-72-325, pp. 50-56, Proceedings of Lightning and Static Electricity Conference, December 12-15, 1972.

13. E. T. Pierce, "Electrostatic Field Changes Due to Lightning Discharges," Quart. J. Roy. Meteorol. Soc., Vol. 81, pp. 211-228 (1955).

14. N. Cianos and E. T. Pierce, "Methods for Lightning Warning and Avoidance," Technical Report 1, Contract 6-73-300H, SRI Project 3057, SRI International, Menlo Park, California (May 1974).

15. N. Cianos, G. N. Oetzel, and E. T. Pierce, "A Technique for Accurately Locating Lightning at Close Ranges," Jour. Appl. Meteor., Vol. II, No. 7, pp. 1120-1127 (October 1972).

16. D. E. Merewether et al., "Electromagnetic Pulse Handbook for Missiles and Aircraft in Flight EMP Interaction 1-1," AFWL TR 73-68, Contract DO AF(29-601)-64-4457 and FY7617-71-10270, Sandia Laboratories, Albuquerque, New Mexico (September 1972).

17. J. A. Plummer, "Transient Analysis Testing of Aircraft to Determine the Electrical Effects of Lightning--Pros and Cons of the Technique," paper presented at the IEEE International Symposium on Electromagnetic Compatibility, Seattle, Washington, August 2-4, 1977.

18. W. G. Butters and D. W. Clifford, "Lightning-Induced Electrical Transient Testing on Aircraft Wiring System," paper presented at the IEEE International Symposium on Electromagnetic Compatibility, Seattle, Washington, August 2-4, 1977.

19. B.J.C. Burrows, C. Luther, and P. Pownall, "Induced Voltages in Full Size Aircraft at 10^{11}A/S," paper presented at the IEEE International Symposium on Electromagnetic Compatibility, Seattle, Washington, August 2-4, 1977.

20. E. F. Vance and W. C. Wadsworth, "Rectangular Coaxial Skin Tester," Technical Memo 24, Contract F29601-69-C-0127, SRI Project 7995, Stanford Research Institute, Menlo Park, California (September 1973).

21 P. Lejay, "Les Perturbations Orageuses du Champe Électrique et Leur Propagation à Grande Distance," thesis, Université de Paris (1926).

22. J. A. Chalmers, Atmospheric Electricity (Pergamon Press, 1957).

1. Report No. NASA CR-159308	2. Government Accession No.	3. Recipient's Catalog No.
4. Title and Subtitle ANALYSIS OF ELECTRICAL TRANSIENTS CREATED BY LIGHTNING		5. Report Date July 1980
		6. Performing Organization Code
7. Author(s) J. E. Nanevicz and E. F. Vance		8. Performing Organization Report No. SRI 4026
		10. Work Unit No.
9. Performing Organization Name and Address SRI International 333 Ravenswood Avenue Menlo Park, California 94025		11. Contract or Grant No. NAS1-13792
		13. Type of Report and Period Covered FINAL REPORT
12. Sponsoring Agency Name and Address National Aeronautics and Space Administration Langley Research Center Hampton, Virginia 23365		14. Sponsoring Agency Code

15. Supplementary Notes

Contract Monitor: Mr. Felix Pitts

16. Abstract

A series of flight tests was conducted using a specially-instrumented NASA Learjet to study the electrical transients created on an aircraft by nearby lightning. The instrumentation included provisions for the time-domain and frequency-domain recording of the electrical signals induced in sensors located both on the exterior and on the interior of the aircraft. The design and calibration of the sensors and associated measuring systems is described together with the results of the flight test measurements.

The results indicate that the concept of providing instrumentation to follow the lightning signal from propagating field, to aircraft skin current, to currents on interior wiring is basically sound. The results of the measurement indicate that the high frequency signals associated with lightning stroke precursor activity are important in generating electromagnetic noise on the interior of the aircraft. Indeed, the signals produced by the precursors are often of higher amplitude and of longer duration than the pulse produced by the main return stroke.

17. Key Words (Suggested by Author(s)) Lightning, Flight Tests, Electromagnetic Interference, Instrumentation, TRIP-76	18. Distribution Statement UNCLASSIFIED - UNLIMITED	
19. Security Classif. (of this report) Unclassified	20. Security Classif. (of this page) Unclassified	21. No. of Pages 101+vi	22. Price*

N-305   For sale by the National Technical Information Service, Springfield, Virginia 22161